
RDKV: Rate-Distortion Bit Allocation for Joint Eviction and Quantization of the KV Cache

Junkai Zhang¹ Hang Guo² Luca Benini¹ Yawei Li¹

¹ ETH Zurich ² Tsinghua University

Abstract

Large language models (LLMs) have shown strong performance across diverse tasks, but their inference with long input contexts is bottlenecked by memory size and bandwidth. The Key-Value (KV) cache size grows linearly with sequence length and needs to be re-read from off-chip high-bandwidth memory (HBM) to on-chip memory at every decoding step, resulting in memory-bound inference. Existing methods reduce the cache by either eviction or quantization, but typically treat the two in isolation. In this paper, we cast KV cache compression as a rate-distortion problem, under which eviction and quantization are two end-points of the same bit allocation scheme. This exposes the need to optimize them jointly, motivating our method, **RDKV** (Rate-Distortion **KV** cache compression). RDKV derives the weight of each token or channel from the distortion that compression induces on the attention computation. Based on these weights, it assigns each token or channel a bit-width ranging from full precision down to zero bits guided by reverse water-filling, applied once after the prefilling stage. Experiments on LongBench, RULER, and InfiniteBench show that RDKV outperforms the best evaluated baseline by 9.1% on average. On LongBench it recovers 97.81% of full-cache accuracy with only 2.48% cache retention. Compared with full-cache FlashAttention-2 decoding, it achieves **4.5**× decode speedup and **1.9**× peak memory reduction with 128K context length, while maintaining comparable performance.

1 Introduction

Large language models (LLMs) [1, 2, 3] have demonstrated strong performance from open-ended generation to complex multi-step reasoning. As these capabilities move into production, the input contexts they require have grown from thousands to hundreds of thousands of tokens. Retrieval-augmented generation [4], multi-document reasoning, and agentic workflows all routinely operate at this scale. At these lengths, inference becomes memory-bound. Transformer decoding stores a Key-Value (KV) pair for every token in every layer. The cache therefore grows linearly with sequence length and reaches tens of gigabytes per request [5]. Because every generated token re-reads this entire cache through the attention computation [6], memory traffic rather than arithmetic sets the per-token decode latency [7]. Reducing the cache footprint without retraining, while preserving generation quality, has thus become a central problem for efficient long-context inference [8, 9].

A growing number of works address this bottleneck by compressing the KV cache after prefill. These methods fall along two axes: eviction and quantization. Eviction methods score each token or channel and keep the top-ranked units at full precision, dropping the rest [10, 11, 12]. Quantization methods retain every token and instead reduce the bit-width [13, 14]. Yet cache units differ widely in importance: a few are critical, most are not. A binary keep-or-evict action leaves no precision tier for the broad middle, while mixed-precision quantization retains every token, including the many that contribute negligibly to the output. Recent analysis shows that combining eviction with quantization outperforms either action alone [15]. Several hybrids route each token among full-precision, low-bit,

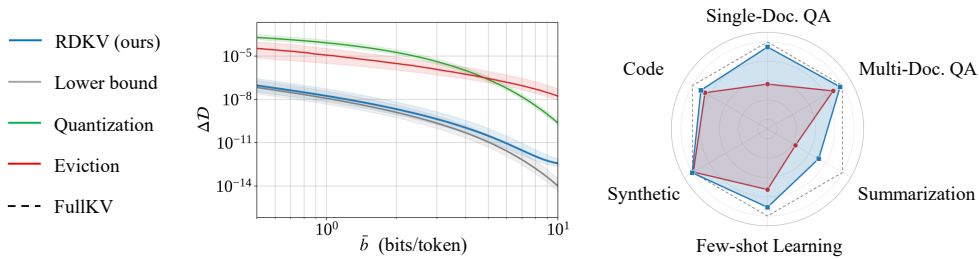


Figure 1: **Left:** Per-sequence weighted distortion $\Delta\mathcal{D} = \sum_u w_u \varepsilon_u(b_u)$ (Eq. (6)) versus average bit-width \bar{b} . Lines: median across sequences; shaded: IQR. *Lower bound:* continuous relaxation (Prop. A.3). **Right:** LongBench score by task category at a per-layer cache budget of 128 FP16-equivalent tokens ($B_{\text{total}} = 128L$), normalized by FullKV; per-task scores in Tab. 1. *Eviction* refers to Ada-SnapKV [26] in the right panel. Model: LLaMA-3.1-8B-Instruct [42].

and evicted states [16, 17]. But their routing scores remain heuristic and the budget ratios are preset or searched before the final assignment. A natural question is whether both the score and the allocation can be derived from a single objective function.

In this paper, we present RDKV, a rate–distortion framework for KV cache compression. RDKV poses a bit-allocation problem: given a fixed bit budget, assign each token in the V cache and each channel in the K cache a bit-width to minimize a weighted distortion. The weight of each token or channel is defined as the deviation in the attention distribution or the attention logit when it is evicted. Reverse water-filling converts these weights into bit-widths, from full precision for critical units down to zero bits (eviction) for negligible ones. Eviction and quantization are thus at the two ends of one allocation curve, and are explored jointly rather than in a staged fashion.

We make three **contributions**. (1) We formulate KV cache compression as a rate–distortion problem. The continuous optimum inherently mixes zero-rate (eviction) and finite-rate (quantization) units. Therefore, approximating this bound requires both actions in the same solver, while restricting to either alone leaves a clear gap, as Fig. 1 (left) shows on calibration data. (2) We instantiate the allocation as a discrete knapsack over hardware-supported bit-widths and solve it via reverse water-filling with Lagrangian relaxation. (3) We realize the resulting mixed-bit cache with TriZone, a packed-decode layout that fuses dequantization into the attention kernel, turning the mixed-bit allocation into actual memory savings. Taken together, Fig. 1 (right) shows the empirical picture: RDKV approaches FullKV’s performance across all six categories while the strong baseline lags consistently.

2 Related Work

Existing KV cache compression methods can be organized by the action they apply: eviction, quantization, or both. Meanwhile, they can also be organized by how the compression target is specified. We adopt the latter axis, distinguishing methods that target a prescribed compression ratio or tier schedule from methods that allocate a given active-cache budget.

Compression-Ratio-Driven Methods. These methods reduce the stored representation of cache entries to reach a target compression ratio. Quantization methods such as KIVI [13], KVQuant [18], ZipCache [14], and KVTuner [19] exploit asymmetric K/V quantization, outlier handling, salient-token preservation, or searched precision configurations to lower the bit-width of stored keys and values. QAQ [20] and MiKV [21] adapt precision by token or KV-pair importance, while AQUA-KV [22] exploits K/V dependencies and quantizes prediction residuals. Several recent hybrids add eviction as the lowest precision tier. HqeKV [17] uses a Tree-structured parzen estimator search (200 trials per setting) to determine the fraction of tokens at each bit-width; ARKV [16] estimates per-layer Original–Quantization ratios from prefill-time attention statistics, with scoring thresholds searched offline. Both methods rely on offline optimization before deployment, with HqeKV searching tier ratios and ARKV searching scoring thresholds.

Budget-Driven Methods. These methods take an active-cache budget as input and decide which units remain available during decoding. KV cache eviction methods score each cache unit and retain the top-ranked subset under a fixed token count. StreamingLLM [23] keeps sink tokens and a recent window. H2O [10], SnapKV [11], Scissorhands [24], and NaCl [25] use attention-derived token scores. AdaKV [26], PyramidKV [27], and CAKE [28] further distribute the budget across heads or layers. Expected Attention [29] estimates future-query scores rather than relying only on the observed window. Recent work sharpens the scoring signal beyond attention weights: CriticalKV [30] optimizes worst-case attention-output perturbation incorporating value states; OBCache [31] applies the Optimal Brain framework [32, 33] to estimate each pair’s impact on the attention output; CAOTE [34] scores via the output error induced by removal; AnDPro [35] projects value states onto anchor directions; ReST-KV [36] stabilizes scores through layer-wise reconstruction and spatial-temporal smoothing. ThinK [12] extends eviction from tokens to key channels.

However, existing budget-driven methods restrict the action to a binary keep-or-drop decision. This restriction leaves no intermediate precision tier for tokens or channels between the two extremes. The framework in Sec. 3 generalizes this budget-driven paradigm: given a total bit budget, it derives per-token or per-channel distortion weights from the attention computation and allocates bit-widths via reverse water-filling. Unlike the ratio-driven hybrids above, eviction and quantization are decided within one allocation problem without offline ratio or threshold optimization.

3 Methodology

Consider a decoder-only transformer [37, 7] with L layers, H_q query heads, H_{kv} KV heads (group size $g = H_q/H_{kv}$) [38], and per-head dimension d . For a prefilled context of T tokens the KV cache per layer comprises $\mathbf{K}, \mathbf{V} \in \mathbb{R}^{H_{kv} \times T \times d}$, with attention weights $a_{\tau,t} = \text{softmax}_t(q_\tau^\top k_t / \sqrt{d})$ and output $o_\tau = \sum_t a_{\tau,t} v_t$. We assign each cache unit u (a token or a channel) a bit-width $b_u \in \mathcal{B} = \{0, 2, 4, 8, 16\}$, from FP16 retention to outright removal, under a total bit budget B . Our goal is to find the allocation $\{b_u^*\}$ that minimizes the distortion introduced to the attention computation under this budget constraint.

In the following, we first quantify the compression cost of each token or channel, and formulate the bit allocation as a rate-distortion problem (Sec. 3.1). We then describe the bit allocation pipeline (Sec. 3.2) and the packed-decode layout that realizes the mixed-bit cache in hardware (Sec. 3.3). Due to space constraints, formal proofs in this section are deferred to Sec. A.

3.1 Rate-Distortion Formulation

To quantify the compression cost of each unit, we analyze the effect of removing a single token or channel from the uncompressed cache. In the V cache, each token enters the output as a single weighted term $a_{\tau,t} v_t$. Removing it perturbs the attention distribution a_τ . In the K cache, persistent channel-wise outliers [13] make the channel the natural compression unit. Zeroing a channel perturbs the logit matrix Z . Because both perturbations are linear, they admit closed-form weights.

Distortion weight in V cache. Consider evicting token t from the V cache of a single head. Because a_τ is produced by softmax, the remaining tokens automatically absorb the freed probability mass. The post-eviction distribution is

$$\hat{a}_{\tau,t} = 0, \quad \hat{a}_{\tau,t'} = \frac{a_{\tau,t'}}{1 - a_{\tau,t}} \quad \text{for } t' \neq t. \quad (1)$$

To measure how much this changes the attention pattern, we use the total variation (TV) distance between a_τ and \hat{a}_τ . It yields the per-token distortion weight:

Proposition 3.1 (Token weight in V cache). *Evicting token t yields $\|a_\tau - \hat{a}_\tau\|_{\text{TV}} = a_{\tau,t}$ for each query τ . The per-token distortion weight, obtained by summing over all queries, is*

$$w_t := \sum_{\tau} a_{\tau,t}. \quad (2)$$

The weight w_t is the total attention that token t receives across all query positions, recovering the cumulative attention widely used as a token-level eviction criterion [10, 11, 26]. In prior work this

quantity serves as a ranking score for binary keep-or-evict decisions. Here it enters the objective as a multiplicative coefficient. Its magnitude therefore affects the allocated bit-width, not merely its rank.

Distortion weight in K cache. An analogous construction applies to the K cache, but with a different partition. Channel c contains the T scalars $\{k_{t,c}\}_{t=1}^T$ across all token positions. Consider removing channel c , i.e., setting $K[:, c]$ to zero. Since each logit entry is the inner product $q_\tau^\top k_t/\sqrt{d}$, zeroing one channel removes the contribution of that coordinate from every entry simultaneously. The resulting deviation in the logit matrix is

$$\delta Z = -\frac{1}{\sqrt{d}} Q[:, c] K[:, c]^\top, \quad (3)$$

and it yields the per-channel distortion weight:

Proposition 3.2 (Channel weight in K cache). *Removing channel c from head h produces a rank-one logit deviation; its spectral norm gives the per-channel distortion weight*

$$w_c := \frac{1}{\sqrt{d}} \|Q[:, c]\|_2 \|K[:, c]\|_2. \quad (4)$$

The weight w_c is the product of the c -th column norms of the query and key matrices: channels whose Q and K columns are both large contribute strongly to the logit and are expensive to remove. This weight coincides with ThinK [12], which arrives at the same expression via Frobenius minimization. As with w_t , the magnitude of w_c shapes its allocated bit-width, not its rank.

Notably, w_t (Eq. (2)) and w_c (Eq. (4)) are both derived from eviction, i.e., the complete removal of a token or channel. However, they extend naturally to quantization because the attention computation is linear in both cache types. Specifically, quantizing a token in the V cache produces the output perturbation $\delta o_\tau = a_{\tau,t} \delta v_t$, so the cost scales with w_t . Similarly, quantizing a channel in the K cache produces a logit perturbation that scales with w_c . The weights w_t and w_c therefore serve as the cost coefficients in the objective function of bit allocation.

Rate-Distortion Aware Bit Allocation. Given these coefficients, the remaining question is how to choose bit-widths b_u under a total budget, where u indexes tokens ($n_u = d$ scalars) or channels ($n_u = T$ scalars). Under Bennett’s high-rate approximation [39], a uniform scalar quantizer with dynamic range R_u achieves per-coordinate root-mean-square error $\sigma_u 2^{-b}$ with $\sigma_u := R_u/(2\sqrt{3})$. Combining the per-unit weights with this per-coordinate error gives the rate-distortion objective

$$\Delta \mathcal{D}(\{b_u\}) = \sum_u w_u \sigma_u 2^{-b_u}, \quad \text{s.t.} \quad \sum_u b_u \leq B. \quad (5)$$

The coefficient $w_u \sigma_u$ combines the distortion weight (w_u) with quantization hardness (σ_u). The Lagrangian solution is a reverse water-filling familiar from channel coding [40, 41]:

Theorem 3.3 (Optimal bit allocation). *The minimizer of Eq. (5) subject to $b_u \geq 0$ is*

$$b_u^* = \left[\log_2 \frac{\ln 2 \cdot w_u \sigma_u}{\lambda} \right]_+,$$

with $\lambda > 0$ chosen so that the budget binds. The water level $\lambda/\ln 2$ induces a phase transition: units with $w_u \sigma_u < \lambda/\ln 2$ receive $b_u^* = 0$, while units above receive finite bit-widths.

Theorem 3.3 reveals that eviction and quantization are not separate actions but two regimes of one allocation curve, selected jointly by the budget B rather than composed under pre-allocated ratios [16]. Tightening the budget B raises λ and pushes more units past the zero-rate boundary into eviction. Loosening it promotes previously evicted units to low-bit retention. The allocator thus navigates eviction and quantization on a single curve, with the budget as the only control knob.

Hardware restricts bit-widths to the discrete set $\mathcal{B} = \{0, 2, 4, 8, 16\}$. We replace Bennett’s curve with an empirical per-coordinate distortion $\varepsilon_u(b)$ calibrated at each $b \in \mathcal{B}$ (see Sec. J), including $b = 0$ for removal, and solve the resulting multiple-choice knapsack problem (MCKP):

$$\{b_u^*\} = \arg \min_{b_u \in \mathcal{B}} \sum_u w_u \varepsilon_u(b_u) \quad \text{s.t.} \quad \sum_u b_u \leq B. \quad (6)$$

Lagrangian relaxation decouples this into independent per-coordinate table lookups. A one-dimensional bisection over λ recovers a feasible primal allocation in $O(U|\mathcal{B}|)$ time, adding negligible latency compared to prefill (Sec. H.1). Weak-duality bounds certify near-optimality (Sec. A).

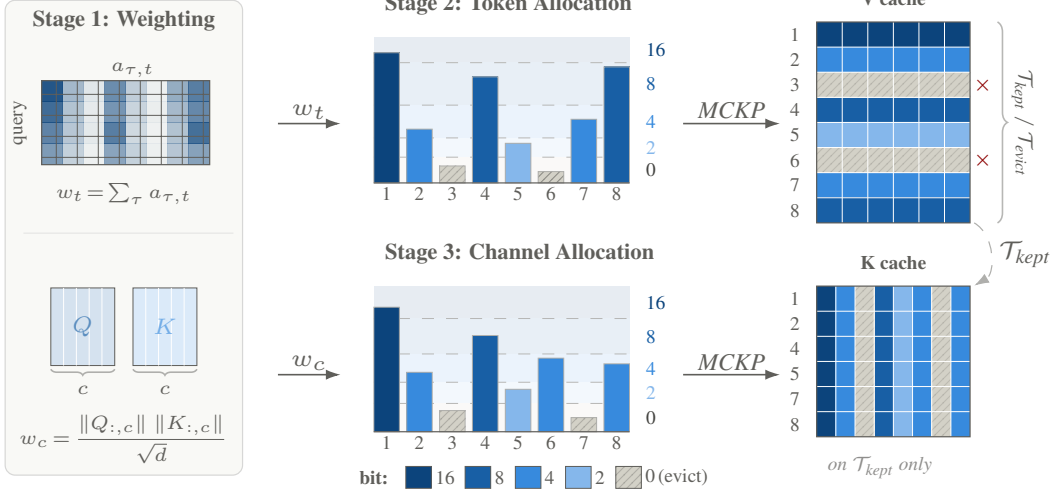


Figure 2: RDKV per-head bit-allocation pipeline (illustrated for 8 tokens and 8 channels). **Stage 1.** Token weights $w_t = \sum_{\tau} a_{\tau,t}$ are derived from the attention matrix, and channel weights w_c from Q/K column norms. **Stage 2.** Reverse water-filling on w_t : four thresholds partition scores into five bit-width zones $\{16, 8, 4, 2, 0\}$. In this example tokens 3 and 6 fall below the lowest threshold and are evicted (hatched rows in V cache). **Stage 3.** The same allocation on w_c assigns per-channel bit-widths to the K cache, which retains only the six kept tokens ($\mathcal{T}_{\text{kept}} = \{1, 2, 4, 5, 7, 8\}$).

3.2 Per-Head Allocation Pipeline

We instantiate the weights and allocation of Sec. 3.1 as a three-stage pipeline (Fig. 2) that runs once after prefill, separately for each layer-head pair (ℓ, h) . Under FP16 reference, a per-head budget of B_{tok} tokens corresponds to $B_{\text{head}} = 2 B_{\text{tok}} d \cdot 16$ total bits, split equally between V and K: $B_V = B_K = \frac{1}{2} B_{\text{head}}$.

Stage 1: Distortion Weight Computation. From the prefill forward pass we compute the token weights w_t (Prop. 3.1) and channel weights w_c (Prop. 3.2), as illustrated in Fig. 2 (a). Both are computed once from the full uncompressed cache: w_t requires only the attention matrix; w_c requires only Q and K column norms, with no value vectors or output residuals needed.

Stage 2: Token Allocation in V Cache. Since each token contains d scalars, the total V budget B_V translates to $\bar{B}_V := B_V/d$ in units of summed bit-widths. Given the token weights w_t and a calibrated distortion table $\varepsilon_V(b)$ (Sec. B), Stage 2 solves the MCKP of Eq. (6), as shown in Fig. 2 (b):

$$\{b_t^V\} = \arg \min_{b_t^V \in \mathcal{B}} \sum_t w_t \varepsilon_V(b_t^V) \quad \text{s.t.} \quad \sum_t b_t^V \leq \bar{B}_V.$$

The output determines $\mathcal{T}_{\text{kept}} := \{t : b_t^V > 0\}$ and its complement $\mathcal{T}_{\text{evict}}$. Retained tokens receive bit-widths in $\{2, 4, 8, 16\}$. Evicted tokens are removed entirely.

Stage 3: Channel Allocation in K Cache. As shown in Fig. 2 (c), Stage 3 distributes the K budget B_K across only the retained tokens $\mathcal{T}_{\text{kept}}$. Each channel contains $|\mathcal{T}_{\text{kept}}|$ scalars, so the budget translates to $\bar{B}_K := B_K/|\mathcal{T}_{\text{kept}}|$:

$$\{b_c^K\} = \arg \min_{b_c^K \in \mathcal{B}} \sum_c w_c \varepsilon_K(b_c^K) \quad \text{s.t.} \quad \sum_c b_c^K \leq \bar{B}_K.$$

A channel assigned $b_c^K = 0$ is removed under the same zero-rate interpretation as token eviction. Across retained tokens, K bit-widths are assigned per-channel independently of the per-token b_t^V . A single token's K and V can therefore carry different bit-widths, the prerequisite for the TriZone layout of Sec. 3.3. Visualization of the resulting bit-width allocations of tokens and channels is in Sec. I.

The V cache is allocated before K because the eviction decision determines which tokens remain in the K cache. Reversing the order would waste K budget on soon-to-be-evicted tokens. The channel weights w_c are reused from Stage 1 without recomputation after V-side eviction, avoiding a second forward pass. The complete pseudocode is given in Sec. C.

3.3 Efficient Packed Decode

The pipeline of Sec. 3.2 produces a mixed-bit cache per (ℓ, h) pair. A mixed-bit allocation alone does not reduce decode cost: if the quantized entries are unpacked to FP16 before the attention kernel reads them, peak HBM usage stays unchanged and the extra dequantization pass adds latency. To translate bit-width savings into actual speedup and memory reduction, the cache must stay packed in HBM while dequantization is fused into the attention computation. The challenge is that tokens within one head now carry different bit-widths, yet GPU kernels require uniform-precision input segments to avoid per-element branching.

We address this by organizing each (ℓ, h) pair into three storage zones that separate packed quantized entries, full-precision retained entries, and newly generated decode tokens. Each zone admits a uniform dequantization path during the attention kernel (Fig. 3; we suppress (ℓ, h) in what follows).

Zone A is the packed old-cache stream: all retained K rows from $\mathcal{T}_{\text{kept}}$, together with the V rows whose $b_t^V \in \{2, 4, 8\}$. Within Zone A, V rows are grouped into uniform-bit segments by b_t^V and K channels by b_c^K (Sec. B). Each segment uses a single dequantization path, avoiding per-element branching. Zone B holds the FP16 V rows for $\mathcal{T}_{V16} := \{t \in \mathcal{T}_{\text{kept}} : b_t^V = 16\}$; their K rows remain in Zone A, since K bit-widths follow the per-channel allocation of Sec. 3.2 rather than b^V . A single token’s K and V can therefore reside in different zones. Zone C appends FP16 K and V for newly generated tokens \mathcal{T}_{new} , growing by one entry per decode step.

At each decode step, the query q_τ attends over retained prefill tokens and newly appended decode tokens. Logits combine the quantized old K with the FP16 new K,

$$z_\tau = q_\tau [\hat{K}_{\mathcal{T}_{\text{kept}}}^\top, K_{\mathcal{T}_{\text{new}}}^\top] / \sqrt{d}, \quad a_\tau = \text{softmax}(z_\tau),$$

and the output decomposes into three value sources:

$$o_\tau = \underbrace{\sum_{t \in \mathcal{T}_{\text{kept}} \setminus \mathcal{T}_{V16}} a_{\tau,t} \hat{v}_t}_{\text{quantized V}} + \underbrace{\sum_{t \in \mathcal{T}_{V16}} a_{\tau,t} v_t}_{\text{FP16 V } (b^V=16)} + \underbrace{\sum_{t \in \mathcal{T}_{\text{new}}} a_{\tau,t} v_t}_{\text{FP16 V (new)}}. \quad (7)$$

The three terms correspond to the three zones: the first reads packed quantized V from Zone A, the second reads FP16 V from Zone B, and the third reads FP16 V from Zone C. Equation (7) is the numerical reference implemented by the packed decode path: dense attention on the compressed cache (\hat{K}, \hat{V}) , with dequantization fused into the attention computation. The latency measurements in Sec. 4 use this implementation. Section B gives layout details including bit-width grouping, padding, and masking.

4 Experiments

Models. We primarily evaluate on LLaMA-3.1-8B-Instruct [42]. Cross-architecture results (Mistral-7B-Instruct-v0.3 [43], Qwen3-4B [44]) and cross-scale results (LLaMA2-13B-Chat [45], Qwen2.5-72B-Instruct [46]) are listed in Sec. D.

Baselines. We compare against four budget-driven methods. SnapKV [11] scores tokens by attention within a recent observation window and retains the top- k per head. Ada-SnapKV [26] (hereafter AdaKV) extends this with adaptive per-head budget allocation. ThinK [12] applies pruning at the channel level of the K cache rather than the token level (paired with SnapKV). SnapKV+ZipCache [11, 14] combines token eviction with post-hoc quantization of the retained cache.

Benchmarks. We evaluate on LongBench [47] (16 tasks covering 6 different task categories), Needle-in-a-Haystack [48] (single-fact retrieval at varying depths), RULER [49] (11 retrieval and reasoning tasks from 4K to 128K), and InfiniteBench [50] (10 tasks with context lengths up to 2M tokens).

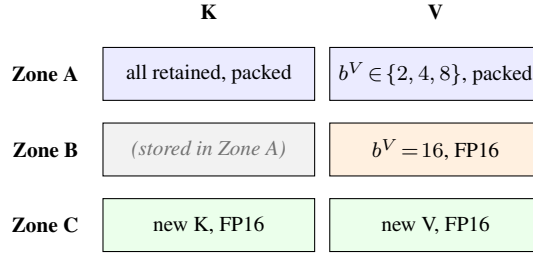


Figure 3: TriZone cache layout for one (ℓ, h) pair. Each zone admits a uniform dequantization path; cell labels show the stored format.

Table 1: Performance on 16 LongBench [47] datasets for LLaMA-3.1-8B-Instruct across cache budgets $B_{\text{total}} \in \{64L, 128L, 256L, 512L, 1024L\}$. Snap+Zip denotes SnapKV [11]+ZipCache [14]. The best result in each row is in **bold**; the second-best is underlined.

Method	Single-Doc QA			Multi-Doc QA			Summarization			Few-shot Learning			Synthetic		Code		Avg.
	NrivQA	Qasper	MF-en	HoprotQA	2WikimQA	Mosique	GovRep	QMSum	MultiNews	TREC	TriviaQA	SAMSum	PCount	PRE	Lcc	RB-P	
<i>LLaMA-3.1-8B-Instruct, $B_{\text{total}} = \text{Full}$</i>																	
FullKV	29.38	44.82	55.46	57.62	49.22	32.80	34.58	25.34	26.90	73.00	91.51	43.64	9.04	99.50	65.24	59.08	48.82
<i>LLaMA-3.1-8B-Instruct, $B_{\text{total}} = 64L$</i>																	
SnapKV[11]	25.20	21.05	39.35	51.69	45.25	26.57	15.06	21.24	14.60	39.00	81.43	36.62	<u>9.00</u>	95.00	54.74	47.41	38.95
AdaKV[26]	24.62	19.62	39.41	50.93	42.13	26.10	16.08	22.17	15.71	39.50	85.62	37.83	<u>9.00</u>	97.50	56.57	50.70	39.59
ThinK[12]	24.93	23.54	45.55	53.54	44.17	27.79	18.38	22.77	18.10	42.00	84.35	38.50	<u>9.00</u>	98.50	55.81	49.22	41.01
Snap+Zip	29.85	<u>32.53</u>	<u>52.16</u>	<u>55.24</u>	<u>46.72</u>	30.60	<u>19.96</u>	<u>22.88</u>	<u>21.26</u>	<u>52.50</u>	<u>90.50</u>	<u>40.03</u>	9.01	75.50	61.01	<u>51.97</u>	<u>43.23</u>
RDKV	<u>28.00</u>	34.47	54.16	55.90	47.45	<u>29.65</u>	23.10	23.78	22.54	59.50	91.76	41.52	8.70	99.17	61.70	54.10	45.97
<i>LLaMA-3.1-8B-Instruct, $B_{\text{total}} = 128L$</i>																	
SnapKV[11]	24.41	24.19	48.91	55.98	45.51	28.41	18.64	22.76	18.72	47.00	88.91	39.41	9.00	98.00	59.14	52.18	42.57
AdaKV[26]	26.35	23.50	51.59	57.11	46.38	28.36	19.68	23.09	19.58	49.50	89.92	40.25	9.00	99.00	60.42	54.59	43.64
ThinK[12]	25.40	30.67	49.96	55.71	46.76	28.47	21.44	23.35	20.83	50.00	89.87	40.97	9.00	99.00	60.18	53.22	44.05
Snap+Zip	<u>29.40</u>	<u>36.64</u>	<u>53.26</u>	<u>57.27</u>	<u>47.23</u>	31.09	<u>22.59</u>	<u>23.66</u>	<u>23.97</u>	<u>61.00</u>	92.00	42.17	8.22	95.50	62.24	53.57	46.24
RDKV	29.45	41.34	55.55	57.39	49.38	<u>30.89</u>	25.55	24.59	24.29	65.00	<u>91.92</u>	<u>41.80</u>	<u>8.75</u>	100.00	62.68	55.41	47.75
<i>LLaMA-3.1-8B-Instruct, $B_{\text{total}} = 256L$</i>																	
SnapKV[11]	26.90	31.27	53.45	56.80	47.97	29.52	21.99	<u>24.34</u>	21.31	55.00	91.41	40.75	8.61	99.00	62.20	55.15	45.35
AdaKV[26]	25.22	32.02	52.51	56.82	47.65	30.71	22.49	23.86	21.78	61.00	91.27	40.92	<u>8.63</u>	99.75	63.42	56.58	45.91
ThinK[12]	26.83	34.14	52.82	56.77	49.14	29.08	23.63	23.47	22.87	61.50	91.51	41.35	8.60	<u>99.50</u>	62.82	55.44	46.22
Snap+Zip	<u>28.02</u>	<u>41.07</u>	<u>54.05</u>	<u>57.74</u>	<u>48.02</u>	31.98	<u>24.27</u>	<u>23.80</u>	<u>24.82</u>	<u>66.00</u>	<u>91.67</u>	42.07	7.90	<u>99.50</u>	61.72	54.18	47.30
RDKV	29.63	44.85	56.33	57.85	49.64	<u>31.73</u>	28.01	24.66	25.66	70.00	91.87	<u>41.79</u>	8.83	<u>99.50</u>	<u>63.27</u>	<u>56.01</u>	48.73
<i>LLaMA-3.1-8B-Instruct, $B_{\text{total}} = 512L$</i>																	
SnapKV[11]	<u>29.68</u>	39.51	55.94	56.94	48.87	30.56	24.31	24.07	23.60	65.50	91.46	41.44	8.57	100.00	<u>64.50</u>	56.58	47.60
AdaKV[26]	27.93	40.26	54.76	<u>56.96</u>	48.68	31.45	25.27	24.09	23.71	<u>69.50</u>	<u>91.96</u>	41.77	<u>8.65</u>	<u>99.50</u>	64.89	57.66	47.94
ThinK[12]	27.96	40.16	55.25	56.85	49.60	31.16	<u>26.00</u>	24.36	24.28	68.00	92.00	41.79	8.63	100.00	64.08	<u>57.30</u>	<u>47.96</u>
Snap+Zip	29.32	<u>41.46</u>	53.15	55.47	46.77	33.26	23.64	<u>24.88</u>	<u>24.89</u>	68.00	91.75	<u>42.32</u>	8.22	<u>99.50</u>	61.75	55.03	47.46
RDKV	30.24	45.67	<u>55.58</u>	57.06	<u>48.95</u>	<u>31.67</u>	30.68	25.06	26.46	72.00	91.83	43.15	8.83	100.00	63.36	57.02	49.22
<i>LLaMA-3.1-8B-Instruct, $B_{\text{total}} = 1024L$</i>																	
SnapKV[11]	29.51	43.17	56.26	57.43	<u>49.18</u>	32.07	27.21	24.63	25.26	69.50	91.70	42.28	8.15	100.00	64.71	58.52	48.72
AdaKV[26]	29.76	<u>43.39</u>	<u>55.82</u>	<u>57.62</u>	48.31	<u>32.35</u>	27.22	24.75	25.18	72.00	91.78	42.12	8.15	100.00	<u>64.56</u>	<u>58.37</u>	<u>48.84</u>
ThinK[12]	27.34	42.48	55.59	57.78	49.17	32.36	<u>28.23</u>	<u>24.82</u>	<u>25.85</u>	<u>71.50</u>	92.50	42.25	8.27	100.00	64.44	58.52	48.82
Snap+Zip	<u>30.23</u>	40.65	54.13	56.06	46.23	31.45	22.84	24.50	24.28	69.00	91.76	44.15	<u>8.61</u>	<u>99.00</u>	60.90	56.38	47.51
RDKV	30.41	44.54	<u>55.82</u>	57.14	49.25	31.77	33.14	25.19	26.92	72.00	<u>91.84</u>	<u>43.90</u>	9.08	100.00	63.56	57.01	49.47

Evaluation Protocol. All methods are evaluated under matched per-layer cache budgets $B_{\text{total}} = nL$ with $n \in \{64, 128, 256, 512, 1024\}$. For RDKV, n is the FP16-equivalent token count reallocated across tokens (V) and channels (K) at bit-widths $\mathcal{B} = \{0, 2, 4, 8, 16\}$. All score-based methods share the same size of observation window and pooling kernel. Further details in Sec. B.

4.1 Main Results

LongBench. LongBench [47] evaluates long-context understanding across 16 tasks spanning single/multi-document QA, summarization, few-shot learning, synthetic, and code. Table 1 reports per-task scores for LLaMA-3.1-8B-Instruct [42] across five cache budgets. RDKV achieves the highest average at every budget: at $B_{\text{total}} = 1024L$ it reaches 49.47, within 0.35 points of FullKV; at $64L$ the lead over the strongest baseline widens to 2.7 points. This reflects a structural advantage of joint allocation. Binary baselines discard every token below the top- k threshold. RDKV instead chooses from a larger action space via reverse water-filling, assigning borderline tokens a low bit-width rather than evicting them. SnapKV+ZipCache [11, 14] also quantizes, but treats eviction and quantization as separate stages rather than two ends of one allocation curve. The advantage spans all six categories; the largest per-task gain appears on GovRep (3–5 points), where attention dispersed across lengthy documents favors mixed-precision over binary eviction. Cross-model results (Mistral-7B [43], Qwen3-4B [44], LLaMA-2-13B [45], Qwen2.5-72B [46]) are in Sec. D.

Needle-In-A-Haystack. Needle-in-a-Haystack [48] tests single-fact retrieval by inserting a target fact at varying depths. Figure 4 compares methods under $B_{\text{total}} = 64L$ at 32k context length. SnapKV [11]

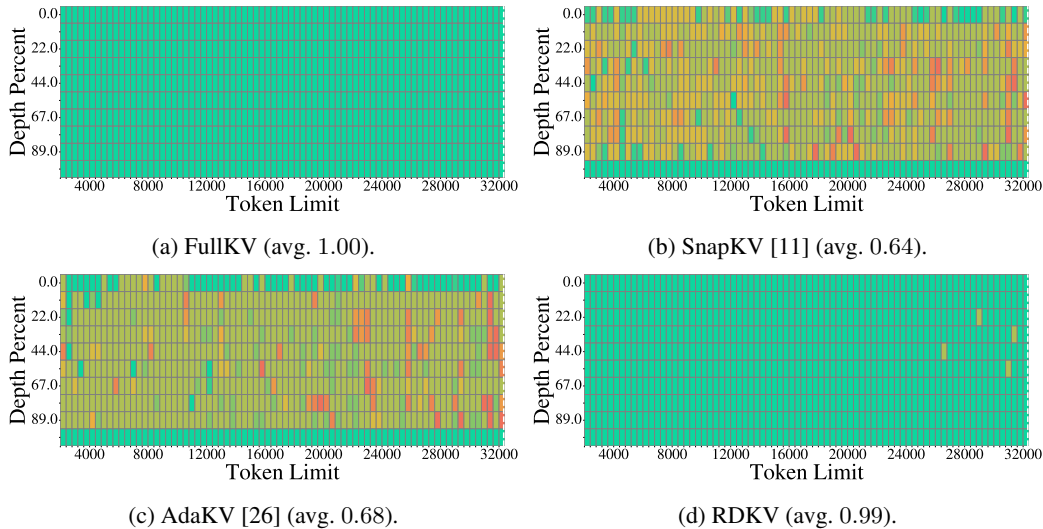


Figure 4: Needle-in-a-Haystack [48] on LLaMA-3.1-8B-Instruct at $B_{\text{total}} = 64L$. RDKV preserves a near-uniform retrieval pattern; SnapKV and AdaKV drop accuracy in mid-depth bands.

Table 2: RULER [49] 11-task average across sequence lengths (LLaMA-3.1-8B-Instruct).

Method	4K	8K	16K	32K	64K	128K
FullKV	98.58	98.88	96.98	90.33	88.49	79.91
SnapKV[11]	89.48	84.75	80.43	75.82	72.77	<u>62.85</u>
AdaKV[26]	<u>92.03</u>	85.49	80.70	75.67	72.47	58.43
ThinK[12]	91.76	86.44	81.45	75.94	72.44	62.85
Snap+Zip	76.49	77.84	76.26	75.05	<u>74.59</u>	62.37
RDKV	98.62	98.61	95.65	88.28	80.07	66.95

Table 3: InfiniteBench [50] 10-task average (LLaMA-3.1-8B-Instruct).

Method	Avg.
FullKV	45.38
SnapKV[11]	37.91
AdaKV[26]	<u>38.06</u>
ThinK[12]	36.73
Snap+Zip	37.76
RDKV	39.46

and AdaKV [26] develop failure bands at intermediate depths where the needle falls below the top- k threshold and is evicted entirely. RDKV assigns the same token a low bit-width instead of discarding it. A 2- or 4-bit copy suffices to recover the answer. RDKV (avg. 0.99) thus maintains near-uniform retrieval close to FullKV (1.00). Further results are in Sec. F.

RULER. RULER [49] evaluates retrieval and reasoning at extreme context lengths, averaging 11 subtasks at sequence lengths from 4k to 128k. Table 2 reports results on LLaMA-3.1-8B-Instruct under $B_{\text{total}} = 1024L$. Eviction-only baselines degrade substantially as context grows, falling over 6 points below FullKV even at 4k and 17 points at 128k. RDKV stays within 1 point of FullKV up to 8k and leads the strongest baseline by 4.1–14.2 points across all lengths, because tokens that a top- k policy would discard are instead retained at low bit-width. Per-task breakdowns are in Sec. E.

InfiniteBench. InfiniteBench [50] spans 10 tasks with sequences exceeding 100k tokens (average $\sim 200k$; the longest task, Zh.QA, reaches $\sim 2M$ tokens). Table 3 reports results on LLaMA-3.1-8B-Instruct under $B_{\text{total}} = 1024L$. RDKV ranks first among compression methods, ahead of AdaKV by 1.40 and SnapKV by 1.55 points, confirming that the allocation advantage persists at ultra-long contexts well beyond the lengths covered by LongBench and RULER. Per-task results are in Sec. G.

4.2 Memory and Latency

Latency. Fig. 5 reports decode latency, peak memory, and the latency-accuracy trade-off on LLaMA-3.1-8B-Instruct from 8K to 256K on a single A100 64GB. Both FullKV and AdaKV [26] use FA2 [51]; reporting FullKV under SDPA would inflate RDKV’s relative speedup to roughly $13\times$. FullKV per-token decode latency grows from 26 ms at 8K to 82 ms at 128K, while RDKV stays flat at ~ 18 ms, a $4.5\times$ speedup at 128K (Fig. 5a), since TriZone’s packed cache size is fixed by B_{total} rather than by T . AdaKV is also at ~ 25 ms under the same token budget, but RDKV is $1.4\times$ faster.

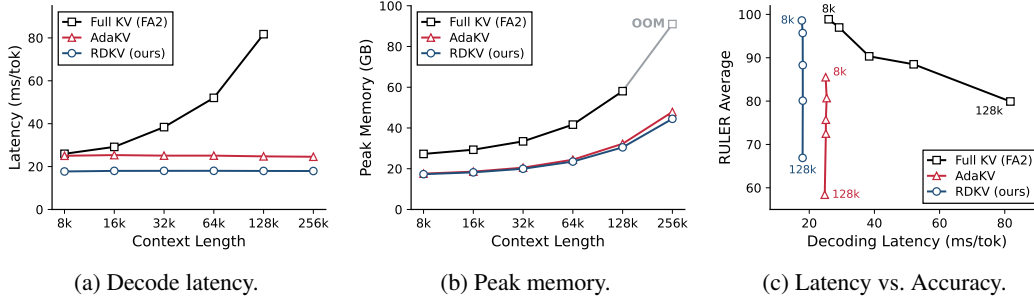


Figure 5: Decode latency, peak memory, and latency-accuracy trade-off for LLaMA-3.1-8B-Instruct from 8K to 256K context length on a single A100 64 GB. Both FullKV and AdaKV use FA2.

Memory. FullKV peak memory grows linearly to 58.1 GB at 128K (Fig. 5b) and OOMs at 256K. RDKV uses 30.5 GB at 128K (1.9 \times reduction vs. FullKV) and 44.5 GB at 256K, running on the same device where FullKV cannot.

Latency-Accuracy Trade-off. Fig. 5c plots latency against RULER accuracy at each context length. RDKV and AdaKV operate at comparable latency, but RDKV is more accurate at every context length: at 128K the gap is 8.5 points (67.0 vs. 58.4). RDKV thus sits strictly above AdaKV on the latency-accuracy Pareto front.

4.3 Ablation Studies

Action Space. We compare four bit-width sets under the same distortion weights and water-filling allocator (Tab. 4, LLaMA-3.1-8B-Instruct, $B_{\text{total}} = 128L$ and $512L$). Removing eviction (Quant-only) costs 8.4 / 8.6 points: the allocator must spend bits on every token, diluting precision for the critical few. Removing quantization (Evict-only) costs 4.9 / 2 points: moderate-importance tokens are discarded entirely when a 2- or 4-bit copy would suffice. Tri-state ($\{0, 4, 16\}$) closes most of the gap (0.5 / 0.2), confirming that *mixing* eviction with quantization matters more than bit-width granularity.

Table 4: Action-space ablation on LongBench average.

Config.	128L	512L
Quant-only	39.06	40.59
Evict-only	42.53	47.18
Tri-state	<u>46.91</u>	<u>49.05</u>
Joint (RDKV)	47.43	49.22

TriZone Packed Decode. Without TriZone (Sec. 3.3), the mixed-bit cache must be unpacked to FP16 before FA2, reading the same HBM as full-precision. Table 5 measured on LLaMA-3.1-8B-Instruct shows the effect: without TriZone, per-token latency is ~ 36 ms at both 16K and 64K; with TriZone, it drops to ~ 18 ms, a 2 \times reduction with bit-identical output. Combined with the smaller cache footprint from mixed-bit allocation, this gives the 4.5 \times decode speedup over FullKV reported in Fig. 5a.

Table 5: TriZone ablation: decode latency (ms/tok).

Config.	16K	64K
RDKV w/ TriZone	17.99	18.02
RDKV w/o TriZone	36.05	36.47

Additional ablation experiments are in Sec. H.

5 Conclusion

We formulate KV cache compression as a rate-distortion problem. The reverse water-filling solution allocates each cache unit a bit-width from $\mathcal{B} = \{0, 2, 4, 8, 16\}$. Eviction emerges as the zero-rate boundary of the same curve as quantization, so sparsification and quantization are selected from a single optimization rather than composed under pre-allocated ratios. A packed-decode layout fuses dequantization into attention, turning the mixed-bit allocation into actual HBM savings. Across LongBench, RULER, and InfiniteBench on five open-source LLMs spanning different architectures and scales, RDKV consistently outperforms the evaluated baselines in accuracy, decoding speed, and peak memory at long context, and reaches 256K on a single A100 64 GB where Full KV does not. Our results show that treating eviction and quantization jointly can improve accuracy at no cost to efficiency. A natural extension is streaming re-budgeting: re-running the allocation during decoding so that the bit assignment adapts to the growing cache instead of being frozen after prefill.

Acknowledgments and Disclosure of Funding

This work was supported by a grant from the Swiss National Supercomputing Centre (CSCS) under project ID lp160 on Alps.

References

- [1] Tom Brown, Benjamin Mann, Nick Ryder, Melanie Subbiah, Jared D Kaplan, Prafulla Dhariwal, Arvind Neelakantan, Pranav Shyam, Girish Sastry, Amanda Askell, et al. Language models are few-shot learners. *Advances in Neural Information Processing Systems*, 33:1877–1901, 2020.
- [2] Josh Achiam, Steven Adler, Sandhini Agarwal, Lama Ahmad, Ilge Akkaya, Florencia Leoni Aleman, Diogo Almeida, Janko Altenschmidt, Sam Altman, Shyamal Anadkat, et al. GPT-4 technical report. *arXiv preprint arXiv:2303.08774*, 2023.
- [3] Aixin Liu, Bei Feng, Bing Xue, Bingxuan Wang, Bochao Wu, Chengda Lu, Chenggang Zhao, Chengqi Deng, Chenyu Zhang, Chong Ruan, et al. DeepSeek-v3 technical report. *arXiv preprint arXiv:2412.19437*, 2024.
- [4] Patrick Lewis, Ethan Perez, Aleksandra Piktus, Fabio Petroni, Vladimir Karpukhin, Naman Goyal, Heinrich Küttler, Mike Lewis, Wen-tau Yih, Tim Rocktäschel, et al. Retrieval-augmented generation for knowledge-intensive NLP tasks. *Advances in Neural Information Processing Systems*, 33:9459–9474, 2020.
- [5] Woosuk Kwon, Zhuohan Li, Siyuan Zhuang, Ying Sheng, Lianmin Zheng, Cody Hao Yu, Joseph Gonzalez, Hao Zhang, and Ion Stoica. Efficient memory management for large language model serving with PagedAttention. In *Proceedings of the 29th Symposium on Operating Systems Principles*, pages 611–626, 2023.
- [6] Tri Dao, Dan Fu, Stefano Ermon, Atri Rudra, and Christopher Ré. FlashAttention: Fast and memory-efficient exact attention with IO-awareness. *Advances in Neural Information Processing Systems*, 35:16344–16359, 2022.
- [7] Reiner Pope, Sholto Douglas, Aakanksha Chowdhery, Jacob Devlin, James Bradbury, Jonathan Heek, Kefan Xiao, Shivani Agrawal, and Jeff Dean. Efficiently scaling transformer inference. *Proceedings of Machine Learning and Systems*, 5:606–624, 2023.
- [8] Haoyang Li, Yiming Li, Anxin Tian, Tianhao Tang, Zhanchao Xu, Xuejia Chen, Nicole Hu, Wei Dong, Qing Li, and Lei Chen. A survey on large language model acceleration based on KV cache management. *arXiv preprint arXiv:2412.19442*, 2024.
- [9] Yanyu Liu, Jingying Fu, Sixiang Liu, Yitian Zou, Shouhua Zhang, and Jiehan Zhou. KV cache compression for inference efficiency in LLMs: A review. In *Proceedings of the 4th International Conference on Artificial Intelligence and Intelligent Information Processing*, pages 207–212, 2025.
- [10] Zhenyu Zhang, Ying Sheng, Tianyi Zhou, Tianlong Chen, Lianmin Zheng, Ruisi Cai, Zhao Song, Yuandong Tian, Christopher Ré, Clark Barrett, et al. H2O: Heavy-hitter oracle for efficient generative inference of large language models. *Advances in Neural Information Processing Systems*, 36:34661–34710, 2023.
- [11] Yuhong Li, Yingbing Huang, Bowen Yang, Bharat Venkitesh, Acyr Locatelli, Hanchen Ye, Tianle Cai, Patrick Lewis, and Deming Chen. SnapKV: LLM knows what you are looking for before generation. *Advances in Neural Information Processing Systems*, 37:22947–22970, 2024.
- [12] Yuhui Xu, Zhanming Jie, Hanze Dong, Lei Wang, Xudong Lu, Aojun Zhou, Amrita Saha, Caiming Xiong, and Doyen Sahoo. ThinK: Thinner key cache by query-driven pruning. *arXiv preprint arXiv:2407.21018*, 2024.
- [13] Zirui Liu, Jiayi Yuan, Hongye Jin, Shaochen Zhong, Zhaozhuo Xu, Vladimir Braverman, Beidi Chen, and Xia Hu. KIVI: A tuning-free asymmetric 2bit quantization for KV cache. *arXiv preprint arXiv:2402.02750*, 2024.

- [14] Yefei He, Luoming Zhang, Weijia Wu, Jing Liu, Hong Zhou, and Bohan Zhuang. ZipCache: Accurate and efficient KV cache quantization with salient token identification. *Advances in Neural Information Processing Systems*, 37:68287–68307, 2024.
- [15] Jiebin Zhang, Dawei Zhu, Yifan Song, Wenhao Wu, Chuqiao Kuang, Xiaoguang Li, Lifeng Shang, Qun Liu, and Sujian Li. More tokens, lower precision: Towards the optimal token-precision trade-off in KV cache compression. *arXiv preprint arXiv:2412.12706*, 2024.
- [16] Jianlong Lei and Shashikant Ilager. ARKV: Adaptive and resource-efficient KV cache management under limited memory budget for long-context inference in LLMs. *arXiv preprint arXiv:2603.08727*, 2026.
- [17] Anonymous. HqeKV: Towards hybrid quantization and eviction for KV cache in long-context LLM inference. In *Submitted to ACL Rolling Review - January 2026*, 2026. under review.
- [18] Coleman Hooper, Sehoon Kim, Hiva Mohammadzadeh, Michael W Mahoney, Yakun S Shao, Kurt Keutzer, and Amir Gholami. KVQuant: Towards 10 million context length LLM inference with KV cache quantization. *Advances in Neural Information Processing Systems*, 37:1270–1303, 2024.
- [19] Xing Li, Zeyu Xing, Yiming Li, Linping Qu, Hui-Ling Zhen, Wulong Liu, Yiwu Yao, Sinno Jialin Pan, and Mingxuan Yuan. KVtuner: Sensitivity-aware layer-wise mixed-precision KV cache quantization for efficient and nearly lossless LLM inference. *arXiv preprint arXiv:2502.04420*, 2025.
- [20] Shichen Dong, Wen Cheng, Jiayu Qin, and Wei Wang. QAQ: Quality adaptive quantization for LLM KV cache. *arXiv preprint arXiv:2403.04643*, 2024.
- [21] June Yong Yang, Byeongwook Kim, Jeongin Bae, Beomseok Kwon, Gunho Park, Eunho Yang, Se Jung Kwon, and Dongsoo Lee. No token left behind: Reliable kv cache compression via importance-aware mixed precision quantization. *arXiv preprint arXiv:2402.18096*, 2024.
- [22] Alina Shutova, Vladimir Malinovskii, Vage Egiazarian, Denis Kuznedelev, Denis Mazur, Nikita Surkov, Ivan Ermakov, and Dan Alistarh. Cache me if you must: Adaptive key-value quantization for large language models. *arXiv preprint arXiv:2501.19392*, 2025.
- [23] Guangxuan Xiao, Yuandong Tian, Beidi Chen, Song Han, and Mike Lewis. Efficient streaming language models with attention sinks. *arXiv preprint arXiv:2309.17453*, 2023.
- [24] Zichang Liu, Aditya Desai, Fangshuo Liao, Weitao Wang, Victor Xie, Zhaozhuo Xu, Anastasios Kyrillidis, and Anshumali Shrivastava. Scissorhands: Exploiting the persistence of importance hypothesis for llm kv cache compression at test time. *Advances in Neural Information Processing Systems*, 36:52342–52364, 2023.
- [25] Yilong Chen, Guoxia Wang, Junyuan Shang, Shiyao Cui, Zhenyu Zhang, Tingwen Liu, Shuo-huan Wang, Yu Sun, Dianhai Yu, and Hua Wu. Nacl: A general and effective kv cache eviction framework for llm at inference time. In *Proceedings of the 62nd Annual Meeting of the Association for Computational Linguistics (Volume 1: Long Papers)*, pages 7913–7926, 2024.
- [26] Yuan Feng, Junlin Lv, Yukun Cao, Xike Xie, and S Kevin Zhou. Ada-KV: Optimizing KV cache eviction by adaptive budget allocation for efficient LLM inference. *arXiv preprint arXiv:2407.11550*, 2024.
- [27] Zefan Cai, Yichi Zhang, Bofei Gao, Yuliang Liu, Yucheng Li, Tianyu Liu, Keming Lu, Wayne Xiong, Yue Dong, Junjie Hu, et al. PyramidKV: Dynamic KV cache compression based on pyramidal information funneling. *arXiv preprint arXiv:2406.02069*, 2024.
- [28] Ziran Qin, Yuchen Cao, Mingbao Lin, Wen Hu, Shixuan Fan, Ke Cheng, Weiyao Lin, and Jianguo Li. Cake: Cascading and adaptive kv cache eviction with layer preferences. *arXiv preprint arXiv:2503.12491*, 2025.
- [29] Alessio Devoto, Maximilian Jeblick, and Simon Jégou. Expected attention: KV cache compression by estimating attention from future queries distribution. *arXiv preprint arXiv:2510.00636*, 2025.

- [30] Yuan Feng, Junlin Lv, Yukun Cao, Xike Xie, and S Kevin Zhou. Identify critical KV cache in LLM inference from an output perturbation perspective. *arXiv preprint arXiv:2502.03805*, 2025.
- [31] Yuzhe Gu, Xiyu Liang, Jiaojiao Zhao, and Enmao Diao. OBCache: Optimal brain KV cache pruning for efficient long-context LLM inference. *arXiv preprint arXiv:2510.07651*, 2025.
- [32] Yann LeCun, John Denker, and Sara Solla. Optimal brain damage. *Advances in Neural Information Processing Systems*, 2, 1989.
- [33] Hang Guo, Yawei Li, and Luca Benini. Optimal brain restoration for joint quantization and sparsification of llms. *arXiv preprint arXiv:2509.11177*, 2025.
- [34] Raghav Goel, Junyoung Park, Mukul Gagrani, Dalton Jones, Matthew Morse, Harper Langston, Mingu Lee, and Chris Lott. Caote: Kv cache selection for LLMs via attention output error-based token eviction. *arXiv preprint arXiv:2504.14051*, 2025.
- [35] Zijie Geng, Jie Wang, Ziqi Liu, Feng Ju, Yiming Li, Xing Li, Mingxuan Yuan, Jianye Hao, Defu Lian, Enhong Chen, et al. Accurate kv cache eviction via anchor direction projection for efficient llm inference. In *The Thirty-ninth Annual Conference on Neural Information Processing Systems*, 2025.
- [36] Yongqi An, Chang Lu, Kuan Zhu, Tao Yu, Chaoyang Zhao, Hong Wu, Ming Tang, and Jinqiao Wang. ReST-KV: Robust KV cache eviction with layer-wise output reconstruction and spatial-temporal smoothing. In *The Fourteenth International Conference on Learning Representations*, 2026.
- [37] Ashish Vaswani, Noam Shazeer, Niki Parmar, Jakob Uszkoreit, Llion Jones, Aidan N Gomez, Łukasz Kaiser, and Illia Polosukhin. Attention is all you need. *Advances in Neural Information Processing Systems*, 30, 2017.
- [38] Joshua Ainslie, James Lee-Thorp, Michiel De Jong, Yury Zemlyanskiy, Federico Lebrón, and Sumit Sanghai. GQA: Training generalized multi-query transformer models from multi-head checkpoints. In *Proceedings of the 2023 Conference on Empirical Methods in Natural Language Processing*, pages 4895–4901, 2023.
- [39] William Ralph Bennett. Spectra of quantized signals. *The Bell System Technical Journal*, 27(3): 446–472, 1948.
- [40] Claude E Shannon et al. Coding theorems for a discrete source with a fidelity criterion. *IRE Nat. Conv. Rec.*, 4(142-163):1, 1959.
- [41] Thomas M. Cover and Joy A. Thomas. *Elements of Information Theory 2nd Edition (Wiley Series in Telecommunications and Signal Processing)*. Wiley-Interscience, July 2006. ISBN 0471241954.
- [42] Aaron Grattafiori, Abhimanyu Dubey, Abhinav Jauhri, Abhinav Pandey, Abhishek Kadian, Ahmad Al-Dahle, Aiesha Letman, Akhil Mathur, Alan Schelten, Alex Vaughan, et al. The Llama 3 herd of models. *arXiv preprint arXiv:2407.21783*, 2024.
- [43] Albert Q. Jiang, Alexandre Sablayrolles, Arthur Mensch, Chris Bamford, Devendra Singh Chaplot, Diego de las Casas, Florian Bressand, Gianna Lengyel, Guillaume Lample, Lucile Saulnier, Léo Renard Lavaud, Marie-Anne Lachaux, Pierre Stock, Teven Le Scao, Thibaut Lavril, Thomas Wang, Timothée Lacroix, and William El Sayed. Mistral 7B, 2023.
- [44] An Yang, Anfeng Li, Baosong Yang, Beichen Zhang, Binyuan Hui, Bo Zheng, Bowen Yu, Chang Gao, Chengen Huang, Chenxu Lv, et al. Qwen3 technical report. *arXiv preprint arXiv:2505.09388*, 2025.
- [45] Hugo Touvron, Louis Martin, Kevin Stone, Peter Albert, Amjad Almahairi, Yasmine Babaei, Nikolay Bashlykov, Soumya Batra, Prajjwal Bhargava, Shruti Bhosale, et al. Llama 2: Open foundation and fine-tuned chat models. *arXiv preprint arXiv:2307.09288*, 2023.

- [46] Qwen, :, An Yang, Baosong Yang, Beichen Zhang, Binyuan Hui, Bo Zheng, Bowen Yu, Chengyuan Li, Dayiheng Liu, Fei Huang, Haoran Wei, Huan Lin, Jian Yang, Jianhong Tu, Jianwei Zhang, Jianxin Yang, Jiaxi Yang, Jingren Zhou, Junyang Lin, Kai Dang, Keming Lu, Keqin Bao, Kexin Yang, Le Yu, Mei Li, Mingfeng Xue, Pei Zhang, Qin Zhu, Rui Men, Runji Lin, Tianhao Li, Tianyi Tang, Tingyu Xia, Xingzhang Ren, Xuancheng Ren, Yang Fan, Yang Su, Yichang Zhang, Yu Wan, Yuqiong Liu, Zeyu Cui, Zhenru Zhang, and Zihan Qiu. Qwen2.5 technical report, 2025.
- [47] Yushi Bai, Xin Lv, Jiajie Zhang, Hongchang Lyu, Jiankai Tang, Zhidian Huang, Zhengxiao Du, Xiao Liu, Aohan Zeng, Lei Hou, et al. LongBench: A bilingual, multitask benchmark for long context understanding. In *Proceedings of the 62nd Annual Meeting of the Association for Computational Linguistics (Volume 1: Long Papers)*, pages 3119–3137, 2024.
- [48] Gregory Kamradt. Needle in a haystack - pressure testing LLMs, 2023.
- [49] Cheng-Ping Hsieh, Simeng Sun, Samuel Kriman, Shantanu Acharya, Dima Rekish, Fei Jia, Yang Zhang, and Boris Ginsburg. RULER: What’s the real context size of your long-context language models? *arXiv preprint arXiv:2404.06654*, 2024.
- [50] Xinrong Zhang, Yingfa Chen, Shengding Hu, Zihang Xu, Junhao Chen, Moo Hao, Xu Han, Zhen Thai, Shuo Wang, Zhiyuan Liu, et al. ∞ bench: Extending long context evaluation beyond 100K tokens. In *Proceedings of the 62nd Annual Meeting of the Association for Computational Linguistics (Volume 1: Long Papers)*, pages 15262–15277, 2024.
- [51] Tri Dao. FlashAttention-2: Faster attention with better parallelism and work partitioning. *arXiv preprint arXiv:2307.08691*, 2023.

A Proofs

This appendix collects the proofs for the results in Sec. 3.1. All quantities below are local to a single layer and KV head (ℓ, h) , with indices suppressed.

Token weight in V cache.

Proof of Prop. 3.1. By definition, $\|a_\tau - \hat{a}_\tau\|_{\text{TV}} = \frac{1}{2} \sum_{t'} |a_{\tau,t'} - \hat{a}_{\tau,t'}|$. The evicted entry contributes $|a_{\tau,t} - 0| = a_{\tau,t}$. Each surviving entry $t' \neq t$ shifts by $|\hat{a}_{\tau,t'} - a_{\tau,t'}| = a_{\tau,t'} \cdot a_{\tau,t} / (1 - a_{\tau,t})$. Summing the surviving terms,

$$\sum_{t' \neq t} a_{\tau,t'} \cdot \frac{a_{\tau,t}}{1 - a_{\tau,t}} = (1 - a_{\tau,t}) \cdot \frac{a_{\tau,t}}{1 - a_{\tau,t}} = a_{\tau,t}.$$

Therefore $\|a_\tau - \hat{a}_\tau\|_{\text{TV}} = \frac{1}{2}(a_{\tau,t} + a_{\tau,t}) = a_{\tau,t}$. Summing over queries, $w_t = \sum_\tau a_{\tau,t}$. \square

Channel weight in K cache.

Proof of Prop. 3.2. Removing channel c sets $K[:, c] = 0$. Since each logit entry is $Z_{\tau,t} = q_\tau^\top k_t / \sqrt{d} = \sum_{c'} q_{\tau,c'} k_{t,c'} / \sqrt{d}$, the logit deviation is $\delta Z = -(1/\sqrt{d}) Q[:, c] K[:, c]^\top$. This is a rank-one matrix uv^\top with $u = Q[:, c] / \sqrt{d}$ and $v = K[:, c]$. A rank-one matrix has a single nonzero singular value $\|u\|_2 \|v\|_2$, so $\|\delta Z\|_2 = \|Q[:, c]\|_2 \|K[:, c]\|_2 / \sqrt{d} = w_c$. \square

Remark A.1. The same expression for w_c obtains under any unitarily invariant norm of δZ (spectral, Frobenius, nuclear, Schatten- p): a rank-one matrix has a single nonzero singular value, so all such norms reduce to $\|u\|_2 \|v\|_2$. In particular, ThinK's Frobenius-based derivation and our spectral-norm derivation yield the same weight.

Bennett high-rate distortion.

Lemma A.2 (Bennett high-rate distortion). *For a uniform scalar quantizer with per-unit dynamic range R_u at bit-width b (high-rate regime), the per-coordinate root-mean-square error is $\sigma_u 2^{-b} + o(2^{-b})$ with $\sigma_u := R_u / (2\sqrt{3})$.*

Proof. With per-unit scale, all n_u coordinates within a unit share a single uniform quantizer of cell width $\Delta = R_u / 2^b$. Bennett's high-rate uniform-cell approximation [39] gives the per-coordinate mean-squared error as $\Delta^2 / 12 + o(\Delta^2) = \sigma_u^2 2^{-2b} + o(2^{-2b})$. Taking the square root yields the per-coordinate RMSE $\sigma_u 2^{-b} + o(2^{-b})$. \square

Optimal allocation.

Proof of Thm. 3.3. The objective $\sum_u w_u \sigma_u 2^{-b_u}$ is strictly decreasing in each b_u , so the budget is active at any optimum: $\sum_u b_u^* = B$. Each summand $w_u \sigma_u 2^{-b_u}$ is convex in b_u (second derivative $(\ln 2)^2 w_u \sigma_u 2^{-b_u} > 0$), so the objective is convex and KKT is sufficient for global optimality. The Lagrangian, with $\lambda \geq 0$ for the budget and $\mu_u \geq 0$ for nonnegativity, is

$$\mathcal{L}(\{b_u\}, \lambda, \{\mu_u\}) = \sum_u w_u \sigma_u 2^{-b_u} + \lambda \left(\sum_u b_u - B \right) - \sum_u \mu_u b_u.$$

Stationarity in b_u gives $-(\ln 2) w_u \sigma_u 2^{-b_u} + \lambda - \mu_u = 0$. For an interior solution ($\mu_u = 0$ by complementary slackness),

$$2^{-b_u} = \frac{\lambda}{\ln 2 \cdot w_u \sigma_u}, \quad \text{i.e.,} \quad b_u = \log_2 \left(\frac{\ln 2 \cdot w_u \sigma_u}{\lambda} \right).$$

When this interior value is negative, the boundary $b_u^* = 0$ activates instead, which occurs iff $w_u \sigma_u < \lambda / \ln 2$. The two cases combine into the $[\cdot]_+$ projection. Since $\sum_u b_u^*(\lambda)$ is monotone non-increasing in λ , the budget equation $\sum_u b_u^*(\lambda) = B$ is solvable by 1D search. \square

Weak duality for discrete allocation.

Proposition A.3 (Weak duality). For $\text{OPT} := \min_{b_u \in \mathcal{B}} \sum_u w_u \varepsilon_u(b_u)$ s.t. $\sum_u b_u \leq B$ with $\mathcal{B} = \{0, 2, 4, 8, 16\}$ and $\varepsilon_u(b)$ the calibration-measured per-coordinate distortion at bit-width b , let $g(\lambda) := \sum_u \min_{b \in \mathcal{B}} [w_u \varepsilon_u(b) + \lambda b] - \lambda B$. Then $g(\lambda) \leq \text{OPT}$ for every $\lambda \geq 0$; when $\{b_u^*(\lambda)\}$ is primal feasible, $\sum_u w_u \varepsilon_u(b_u^*(\lambda))$ is an upper bound.

Proof. For any feasible $\{b_u\}$ and $\lambda \geq 0$,

$$\sum_u w_u \varepsilon_u(b_u) \geq \sum_u w_u \varepsilon_u(b_u) + \lambda \left(\sum_u b_u - B \right) \geq \sum_u \min_{b \in \mathcal{B}} [w_u \varepsilon_u(b) + \lambda b] - \lambda B = g(\lambda),$$

using $\sum_u b_u - B \leq 0$ in the first inequality and per-unit minimization in the second. Taking minimum over feasible primals yields $\text{OPT} \geq g(\lambda)$. Conversely, any feasible $\{b_u^*(\lambda)\}$ satisfies $\sum_u w_u \varepsilon_u(b_u^*(\lambda)) \geq \text{OPT}$ by definition. \square

B Detailed Implementation

This appendix expands on the implementation details abbreviated in Sec. 4.

Prefill stage. Probe-based score computation, rate-distortion bit allocation, and TriZone packing are performed once at the end of prefill, on the same hidden states already produced by the forward pass. The probe shares the SnapKV observation window of size $S_w = 32$ and pooling kernel $w = 5$ across all eviction-style baselines (SnapKV, AdaKV, ThinK, SnapKV+ZipCache) to ensure that score-based comparisons isolate the indicator and the allocation, not the probe geometry. The bit-width set is fixed to $\mathcal{B} = \{0, 2, 4, 8, 16\}$. The K/V budget is split equally, $B^V = B^K = \frac{1}{2} B_{\text{head}}$, as a symmetric default validated by the ablation in Sec. H.2, which shows that $r_K = 0.5$ consistently achieves the highest average score across budget levels.

Calibration. The empirical per-coordinate distortion table $\varepsilon_u(b)$ is estimated on calibration sequences drawn from the prefill prefixes of the LongBench tasks. We use 32 sequences (truncated to 4k tokens each) to estimate $\varepsilon_u(b)$ for each $b \in \{2, 4, 8\}$ at the per-token (V) and per-channel (K) granularities. The estimate at $b = 0$ is computed from the same sample but refers to outright removal rather than quantization, as discussed in Sec. 3. Calibration is performed once per (ℓ, h) slice and cached to disk.

Lagrangian search. The MCKP (Prop. A.3) is solved by one-dimensional bisection on λ . At each step we evaluate the per-element minimizer $b_u^*(\lambda) = \arg \min_{b \in \mathcal{B}} w_u \varepsilon_u(b) + \lambda b$ via table lookup, and bisect on λ until the average bit budget $\frac{1}{|U|} \sum_u b_u^*(\lambda)$ matches the target B within a relative tolerance of 10^{-2} , or after at most 64 bisection steps. The resulting allocation is treated as the final b_u^* .

Hardware. All models up to 8B parameters (LLaMA-3.1-8B-Instruct, Mistral-7B-Instruct-v0.3, Qwen3-4B) run on a single NVIDIA A100 64 GB GPU. LLaMA-2-13B-Chat and Qwen2.5-72B-Instruct run on NVIDIA GH200 96 GB GPUs; Qwen2.5-72B uses 2-GPU tensor parallelism. Decoding latency and peak memory measurements (Sec. 4, Fig. 5) are collected on the A100 64 GB.

Baseline implementations. SnapKV and AdaKV use the official `kvpress` implementations. ThinK [12] and ZipCache [14] use their respective official open-source code. SnapKV+ZipCache combines the `kvpress` SnapKV with the official ZipCache mixed-precision quantizer, with no code modifications. All baselines use the default hyperparameters recommended by their respective authors. All methods receive the same prefill probe ($S_w = 32$, $w = 5$) so that any difference in the resulting weights is attributable to the indicator, not the calibration window.

Baseline selection rationale. For the eviction+quantization slot we compose SnapKV [11] with ZipCache [14] rather than adopting QPruningKV [15] directly. QPruningKV focuses on discussing the combination of existing eviction and quantization methods rather than proposing a new joint algorithm. In addition, the quantization methods it adopts assign precision only at layer level [13], a coarse granularity consistently outperformed by token-level alternatives such as ZipCache [14].

TriZone packed layout. Within Zone A (Sec. 3.3), V rows are sorted by b_t^V into three contiguous sub-segments, each with a distinct byte-packing convention over the head dimension d : 2-bit uses *quarter-split* packing (four channels per byte at bit offsets 0, 2, 4, 6; $d/4$ packed bytes per row), 4-bit uses *half-split* packing (two channels per byte at offsets 0, 4; $d/2$ bytes per row), and 8-bit stores one channel per byte directly. Each sub-segment admits a single shift-and-mask dequantization path with no per-element branching. K channels within each retained row follow the per-channel allocation b_c^K :

channels are sorted by bit-width into three analogous 2/4/8-bit segments along the channel axis, and the query q_τ is permuted to the same sorted order once at the end of prefill.

K-cache dequantization fusion. Per-channel quantization encodes channel c of the retained K cache as $\hat{k}_{t,c} = s_c (\tilde{k}_{t,c} - z_c)$, where s_c, z_c are the per-channel scale and zero-point and $\tilde{k}_{t,c} \in \{0, \dots, 2^{b^k} - 1\}$ is the raw integer code. The kernel avoids materializing a dequantized FP16 tile by rewriting the dot product as

$$q_\tau^\top \hat{k}_t = \sum_c (s_c q_{\tau,c}) \tilde{k}_{t,c} - \sum_c s_c z_c q_{\tau,c}.$$

The scaled query $\tilde{q}_c = s_c q_{\tau,c}$ is computed once per decode step and cast to FP16 for the tensor-core matrix multiply. Raw codes $\tilde{k}_{t,c}$ are cast exactly to FP16 (all values ≤ 255) and serve as the right operand. The second sum is a per-query-head bias independent of t , subtracted once after the dot product accumulates over all retained tokens. This avoids one write/read pass of $|\mathcal{T}_{\text{kept}}| \times d$ FP16 values per decode step.

Padding and alignment. Bit-packing imposes alignment constraints on K-channel segment sizes: the 2-bit segment is zero-padded so that the channel count is a multiple of 4 (four channels per packed byte), and the 4-bit segment is padded to a multiple of 2. Padded channels receive $s_c = z_c = 0$ and thus contribute zero to both the dot product and the bias term. The 8-bit segment has no alignment constraint. V sub-segments are padded analogously along d .

Masking. Two boolean masks guard out-of-range accesses in the Triton kernels: a token-axis mask ($i < T_{\text{eff}}$) zeroes loads beyond the effective token count, and a channel-axis mask ($j < N_{\text{ch}}$, K-side only) zeroes loads beyond the true segment width. Since padded channels have $s_c = z_c = 0$, masked positions dequantize to zero and contribute nothing to the final result.

C Algorithm

Algorithm 1 summarizes the full RDKV pipeline executed once at the end of prefill. The algorithm takes the prefill KV cache and a per-head bit budget as input, and produces the TriZone packed cache used during decoding.

MCKP (Alg. 2) solves the multiple-choice knapsack via Lagrangian bisection on λ . For each candidate λ , every unit independently picks the bit-width minimizing its cost $w_u \varepsilon_u(b) + \lambda b$. The bisection terminates when the average bit-width is within tolerance of the budget.

D Additional Experiments on LongBench

In this section, we provide comprehensive experimental results on LongBench [47], a benchmark focused on long-context understanding with 16 tasks spanning single-document QA, multi-document QA, summarization, few-shot learning, synthetic retrieval, and code completion. We perform detailed evaluations with cache budgets ranging from $64L$ to $1024L$ on four additional models beyond the primary LLaMA-3.1-8B-Instruct reported in Sec. 4.1: Mistral-7B-Instruct-v0.3 [43] and Qwen3-4B [44] to test cross-architecture generality, and LLaMA-2-13B-Chat [45] and Qwen2.5-72B-Instruct [46] (2-GPU tensor parallelism) to test cross-scale generality. All methods share the same probe configuration ($S_w = 32, w = 5$) so that any performance difference is attributable to the indicator and allocation, not the probe geometry.

Tables 6 to 8 present the detailed per-task scores. Overall, RDKV achieves the highest average at every (model, budget) combination—without architecture-specific tuning. The advantage is largest under aggressive compression: at $B_{\text{total}} = 64L$, RDKV leads the strongest baseline by 1.5/5.5/2.7 points on Mistral-7B/Qwen3-4B/LLaMA-3.1-8B, because water-filling retains moderate-importance tokens at low bit-width rather than evicting them entirely. At $B_{\text{total}} = 1024L$ it recovers 98.6–99.4% of FullKV across models; on the two larger models (LLaMA-2-13B, Qwen2.5-72B) the recovery reaches 99.5–99.6% already at $B_{\text{total}} = 512L$. The consistency across architectures and scales suggests that the distortion weights (Sec. 3) capture a model-agnostic signal, enabling the allocation to transfer without modification.

Algorithm 1 RDKV: Rate-Distortion KV Cache Compression

Require: Prefill KV cache $K^{(\ell)}, V^{(\ell)}$ for each layer ℓ ; per-head budget B_{head} ; observation window size S_w ; pooling kernel w ; bit-width set $\mathcal{B} = \{0, 2, 4, 8, 16\}$; empirical distortion tables $\varepsilon^K(b), \varepsilon^V(b)$

Ensure: TriZone packed cache for each (ℓ, h)

```
1: for each layer  $\ell = 1, \dots, L$  do
2:   // Stage 1: Weight computation
3:    $A \leftarrow \text{Softmax}(Q_{[\tau-S_w:\tau]}^{(\ell)} K^{(\ell)\top} / \sqrt{d})$ 
4:   for each KV head  $h = 1, \dots, H_{\text{KV}}$  do
5:      $w_t^{(h)} \leftarrow \sum_{\tau, g} a_{\tau, g, t}^{(h)}$  for all  $t$  ▷ token weight in V cache
6:      $w_t^{(h)} \leftarrow \text{AvgPool1d}(w_t^{(h)}, w)$ 
7:      $w_c^{(h)} \leftarrow \frac{1}{\sqrt{d}} \|Q_{:,c}^{(h)}\|_2 \cdot \|K_{:,c}^{(h)}\|_2$  for all  $c$  ▷ channel weight in K cache
8:   end for

9:   // Stage 2: V-side token allocation (per head)
10:   $B^V \leftarrow \frac{1}{2} B_{\text{head}}; \bar{B}^V \leftarrow B^V / d$ 
11:  for each KV head  $h$  do
12:     $\{b_t^V\}_h \leftarrow \text{MCKP}(w_t^{(h)}, \varepsilon^V, \bar{B}^V / T)$ 
13:     $\mathcal{T}_{\text{kept}}^{(h)} \leftarrow \{t : b_t^V > 0\}$ 
14:  end for

15:  // Stage 3: K-side channel allocation (per head)
16:   $B^K \leftarrow \frac{1}{2} B_{\text{head}}$ 
17:  for each KV head  $h$  do
18:     $k_{\text{avg}}^{(h)} \leftarrow B^K / (|\mathcal{T}_{\text{kept}}^{(h)}| \cdot d)$ 
19:     $\{b_c^K\}_h \leftarrow \text{MCKP}(w_c^{(h)}, \varepsilon^K, k_{\text{avg}}^{(h)})$ 
20:  end for

21:  // Stage 4: TriZone packing
22:  for each KV head  $h$  do
23:    Sort  $\mathcal{T}_{\text{kept}}^{(h)}$  by  $b_t^V$  into sub-segments  $\mathcal{S}_2, \mathcal{S}_4, \mathcal{S}_8$ 
24:    Sort channels by  $b_c^K$  into segments; permute  $q$  to match
25:    Quantize and byte-pack V sub-segments  $\rightarrow$  Zone A (V)
26:    Quantize and byte-pack K rows of  $\mathcal{T}_{\text{kept}}^{(h)} \rightarrow$  Zone A (K)
27:    Store  $\{t : b_t^V = 16\}$  V rows in FP16  $\rightarrow$  Zone B
28:  end for
29: end for
```

E Additional Experiments on RULER

In this section, we present a detailed evaluation of RDKV on the various subtasks of the RULER benchmark [49]. RULER is specifically designed to assess core long-context capabilities through a diverse suite of tasks. The retrieval suite includes four variants of needle-in-a-haystack tests: Single-Needle (S-NIAH-1/2/3) at increasing difficulty, Multi-Key (MK-NIAH-1/2/3), Multi-Query (MQ-NIAH), and Multi-Value (MV-NIAH), which evaluate recall accuracy under diverse distractor settings and query formulations. Beyond retrieval, Variable Tracking (VT) measures multi-hop reasoning by requiring models to resolve transitive variable references scattered throughout the input. Lastly, the aggregation tasks Common Word Extraction (CWE) and Frequent Word Extraction (FWE) test the ability to compress and synthesize high-density signal distributed across long contexts. These tasks collectively pose distinct challenges for context retention, salience estimation, and compositional reasoning.

We evaluate RDKV on LLaMA-3.1-8B-Instruct with $B_{\text{total}} = 2048L$, across input lengths from 4k to 128k tokens. The evaluation compares RDKV with SnapKV, AdaKV, ThinK, SnapKV+ZipCache, and FullKV (oracle).

Algorithm 2 MCKP: Lagrangian Bisection Knapsack Solver

Require: Weights $\{w_u\}$; distortion table $\varepsilon(b)$; target average bits \bar{b} ; bit-width set \mathcal{B} ; tolerance δ ; max iterations I

Ensure: Bit-width assignment $\{b_u^*\}$

```
1:  $\lambda_{lo} \leftarrow 0$ ;  $\lambda_{hi} \leftarrow \max_u w_u$ 
2: for  $i = 1, \dots, I$  do
3:    $\lambda \leftarrow (\lambda_{lo} + \lambda_{hi})/2$ 
4:   for each unit  $u$  do
5:      $b_u^* \leftarrow \arg \min_{b \in \mathcal{B}} w_u \varepsilon(b) + \lambda b$ 
6:   end for
7:    $\bar{b}_{cur} \leftarrow \text{mean}(\{b_u^*\})$ 
8:   if  $|\bar{b}_{cur} - \bar{b}|/\bar{b} < \delta$  then
9:     return  $\{b_u^*\}$ 
10:  else if  $\bar{b}_{cur} > \bar{b}$  then
11:     $\lambda_{lo} \leftarrow \lambda$ 
12:  else
13:     $\lambda_{hi} \leftarrow \lambda$ 
14:  end if
15: end for
16: return  $\{b_u^*\}$ 
```

As reported in Tab. 9, RDKV consistently achieves the highest average accuracy across all context lengths. At 4k tokens, RDKV matches FullKV (98.59 vs. 98.58), while the best eviction baseline (ThinK) reaches 98.11. As context length increases, the gap widens: at 64k, RDKV leads with 83.20 vs. 78.73 for the next best method (AdaKV), a 4.5-point margin. A breakdown by task category clarifies the source of the advantage. On S-NIAH-3—the hardest single-needle retrieval variant—RDKV is the only method that stays above 99% from 4k through 64k; SnapKV and AdaKV drop to 89.80/92.60 at 64k and to 50.80/47.80 at 128k, whereas RDKV still reaches 99.80 and 93.80, respectively. The CWE aggregation task at 16k illustrates a complementary advantage: eviction discards low-attention tokens that carry the frequency signal, yielding 46–55 for the baselines; RDKV retains these tokens at low bit-width and scores 77.26, a 22-point improvement over the next best method.

Comparison with HqeKV. HqeKV [17] is a concurrent method that also combines eviction and quantization, but fixes the tier ratios rather than deriving them from a single allocation curve. Table 10 compares RDKV and HqeKV on the 11 RULER tasks at $B_{total} = 1024L$ across three context lengths (16k, 32k, 64k) on LLaMA-3.1-8B-Instruct. RDKV leads at every context length, with the gap widening from +1.8 points at 32k to +5.3 at 16k and +5.0 at 64k. The advantage is concentrated on tasks where the allocation granularity matters most: on CWE, RDKV leads by +49.9 / +22.0 / +6.5 points across the three lengths; on MV-NIAH, by +3.4 / +7.4 / +12.1; on MQ-NIAH, by +2.7 / +5.3 / +12.2. HqeKV outperforms RDKV on FWE at 32k and 64k and on MK-NIAH-3 at 32k, where its fixed high-precision tier retains more tokens at full bit-width; RDKV’s water-filling allocator trades off these tokens for finer-grained precision elsewhere.

F Additional Experiments on Needle-in-a-Haystack

Figure 6 extends the Needle-in-a-Haystack evaluation of Sec. 4.1 to a larger cache budget $B_{total} = 128L$. Even with the relaxed budget, SnapKV and AdaKV still exhibit failure bands at intermediate depths (11–89%) for longer contexts: a needle that does not rank among the top- k tokens is evicted regardless of the budget headroom. RDKV preserves a near-uniform success pattern comparable to FullKV; the residual misses concentrate at depths and lengths where FullKV itself begins to lose recall.

Table 6: Performance on 16 LongBench datasets for Mistral-7B-Instruct-v0.3 across cache budgets $B_{\text{total}} \in \{64L, 128L, 256L, 512L, 1024L\}$. Snap+Zip denotes SnapKV+ZipCache. The best result in each row is in **bold**; the second-best is underlined.

Method	Single-Doc QA			Multi-Doc QA			Summarization			Few-shot Learning			Synthetic	Code		Avg.	
	NrivQA	Qasper	MF-en	HotpotQA	2WikiMQA	Musique	GovRep	QMSum	MultiNews	TREC	TriviaQA	SAMSum	PCount	Pre	Lcc		RB-P
<i>Mistral-7B-Instruct-v0.3, $B_{\text{total}} = \text{Full}$</i>																	
FullKV	25.91	38.13	49.62	52.07	39.03	28.10	34.11	25.73	26.47	76.00	88.59	47.46	7.01	98.00	61.58	62.34	47.51
<i>Mistral-7B-Instruct-v0.3, $B_{\text{total}} = 64L$</i>																	
SnapKV	17.53	17.78	32.36	40.94	30.84	19.34	16.27	20.33	13.77	38.00	87.64	38.80	5.00	76.50	48.46	47.72	34.45
AdaKV	17.33	18.43	34.33	42.13	31.16	21.08	16.79	20.64	14.23	38.00	88.18	39.61	3.50	83.00	51.28	48.93	35.54
ThinK	20.27	24.90	40.42	45.00	33.54	21.44	19.83	21.26	18.45	39.50	87.94	40.66	3.00	83.00	53.19	51.51	37.74
Snap+Zip	<u>22.80</u>	<u>25.83</u>	47.55	47.38	35.23	24.03	<u>21.54</u>	<u>21.59</u>	<u>21.61</u>	<u>55.00</u>	<u>89.05</u>	<u>44.84</u>	4.00	<u>88.00</u>	<u>56.59</u>	<u>56.61</u>	<u>41.35</u>
RDKV	24.70	29.46	<u>47.51</u>	<u>46.48</u>	<u>34.37</u>	<u>22.73</u>	23.40	23.23	22.73	60.00	89.07	44.99	<u>4.50</u>	96.00	57.78	58.19	42.82
<i>Mistral-7B-Instruct-v0.3, $B_{\text{total}} = 128L$</i>																	
SnapKV	21.25	22.92	42.30	44.75	33.34	21.24	21.00	21.37	19.30	44.50	89.35	42.47	4.50	91.00	55.98	54.12	39.34
AdaKV	21.97	23.31	46.28	46.67	34.52	21.47	20.92	21.85	19.71	49.00	<u>89.19</u>	42.63	6.50	91.50	56.41	55.60	40.47
ThinK	21.90	29.83	48.32	47.25	34.76	23.27	21.73	<u>22.37</u>	21.18	47.50	88.36	43.10	5.00	93.00	57.62	56.39	41.35
Snap+Zip	<u>23.62</u>	<u>32.30</u>	<u>48.55</u>	50.23	<u>35.41</u>	26.96	<u>24.22</u>	22.23	<u>23.58</u>	<u>67.50</u>	88.63	<u>45.19</u>	<u>5.50</u>	92.00	<u>59.01</u>	<u>58.30</u>	<u>43.95</u>
RDKV	25.61	33.76	48.58	<u>48.65</u>	36.19	<u>25.37</u>	25.39	24.14	24.14	70.00	89.18	45.52	5.00	97.50	59.30	59.69	44.88
<i>Mistral-7B-Instruct-v0.3, $B_{\text{total}} = 256L$</i>																	
SnapKV	24.37	29.08	47.68	48.14	34.66	24.45	23.17	23.24	22.37	57.00	88.85	44.36	6.00	<u>96.50</u>	59.32	57.98	42.95
AdaKV	24.71	30.19	48.31	49.08	34.69	26.03	23.13	23.46	22.19	66.00	<u>88.93</u>	44.57	4.50	<u>96.50</u>	59.38	59.67	43.83
ThinK	24.82	31.21	50.22	50.79	35.00	23.70	23.75	23.55	23.17	66.00	89.61	43.90	<u>5.50</u>	94.50	59.37	59.04	44.01
Snap+Zip	<u>27.21</u>	<u>36.41</u>	<u>49.96</u>	<u>50.54</u>	37.33	25.04	25.82	23.87	24.70	<u>72.50</u>	88.94	45.01	6.00	<u>96.00</u>	<u>60.58</u>	<u>62.08</u>	<u>45.75</u>
RDKV	26.00	<u>35.68</u>	<u>49.89</u>	49.11	<u>35.50</u>	<u>25.99</u>	27.78	24.48	<u>25.22</u>	73.50	88.58	46.40	6.00	97.00	<u>59.49</u>	60.60	45.70
<i>Mistral-7B-Instruct-v0.3, $B_{\text{total}} = 512L$</i>																	
SnapKV	25.89	32.99	48.59	50.39	<u>36.72</u>	26.24	24.86	23.81	24.17	69.00	89.28	45.39	6.00	97.50	60.21	61.03	45.13
AdaKV	26.04	33.06	50.75	50.29	35.81	<u>26.58</u>	25.03	23.39	23.65	71.50	88.86	46.03	6.00	97.50	60.74	62.25	45.47
ThinK	<u>27.21</u>	<u>36.41</u>	<u>49.96</u>	<u>50.54</u>	37.33	25.04	25.82	23.87	24.70	<u>72.50</u>	88.94	45.01	6.00	<u>96.00</u>	<u>60.58</u>	<u>62.08</u>	45.75
Snap+Zip	27.57	35.17	48.23	51.43	36.70	25.40	<u>28.66</u>	<u>24.37</u>	<u>25.61</u>	75.50	89.01	<u>46.09</u>	6.00	95.50	60.34	60.70	<u>46.02</u>
RDKV	26.06	37.26	49.62	50.07	36.58	26.99	30.48	25.14	26.23	75.50	<u>89.08</u>	46.77	<u>5.50</u>	<u>96.50</u>	59.14	60.58	46.34
<i>Mistral-7B-Instruct-v0.3, $B_{\text{total}} = 1024L$</i>																	
SnapKV	26.05	35.63	50.05	50.39	36.44	<u>27.40</u>	27.24	23.97	25.22	73.00	89.19	45.84	6.00	98.50	<u>61.42</u>	61.55	46.12
AdaKV	26.31	36.49	49.95	51.76	37.37	<u>27.07</u>	27.11	<u>24.84</u>	25.01	73.00	<u>89.03</u>	45.83	5.50	98.50	61.03	62.35	46.32
ThinK	27.97	38.68	<u>49.96</u>	49.97	38.69	25.28	28.05	24.57	25.75	<u>74.00</u>	88.72	45.83	6.50	95.00	61.67	<u>61.85</u>	46.41
Snap+Zip	26.41	37.75	48.90	<u>51.54</u>	35.26	25.74	<u>30.97</u>	24.25	<u>26.07</u>	76.00	88.70	<u>46.25</u>	<u>6.06</u>	95.50	59.18	60.71	46.21
RDKV	<u>27.00</u>	<u>37.96</u>	49.88	50.56	<u>37.63</u>	28.20	32.33	25.05	26.57	76.00	88.48	47.88	5.00	<u>97.50</u>	59.35	60.40	46.86

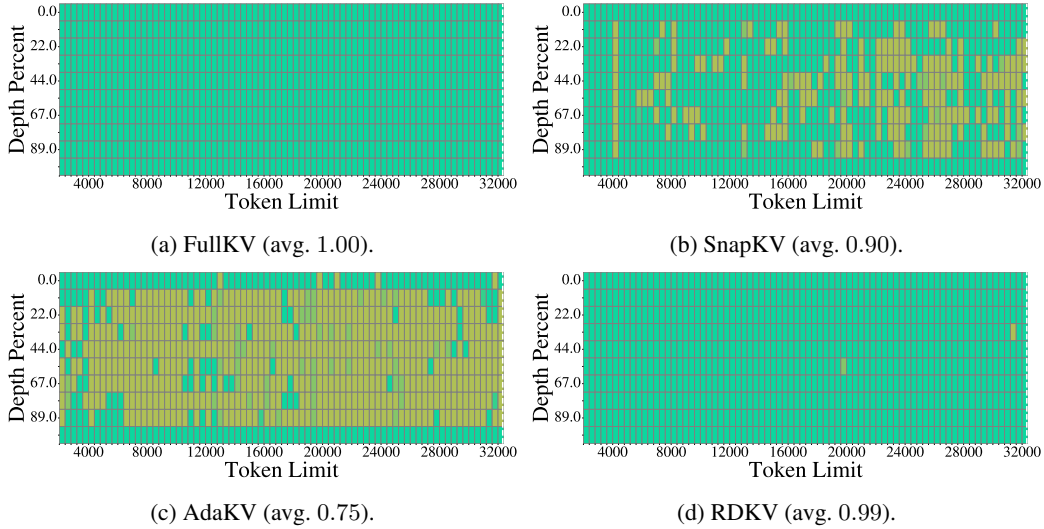


Figure 6: Needle-in-a-Haystack on LLaMA-3.1-8B-Instruct at $B_{\text{total}} = 128L$ and context length up to 32k. Green denotes successful retrieval; warmer colours denote partial or complete failure.

Table 7: Performance on 16 LongBench datasets for Qwen3-4B-Instruct-2507 across cache budgets $B_{\text{total}} \in \{64L, 128L, 256L, 512L, 1024L\}$. Snap+Zip denotes SnapKV+ZipCache. The best result in each row is in **bold**; the second-best is underlined.

Method	Single-Doc QA			Multi-Doc QA			Summarization			Few-shot Learning			Synthetic		Code		Avg.
	NrtvQA	Qasper	MF-en	HotpotQA	2WikiMQA	Mustique	GovRep	QMSum	MultiNews	TREC	TriviaQA	SAMSum	PCCount	Pre	Lcc	RB-P	
<i>Qwen3-4B-Instruct-2507, B_{total} = Full</i>																	
FullKV	27.96	44.61	49.84	58.84	43.27	25.54	30.64	22.56	24.06	74.50	87.15	45.36	2.15	100.00	64.69	57.56	47.42
<i>Qwen3-4B-Instruct-2507, B_{total} = 64L</i>																	
SnapKV	16.95	26.10	35.04	43.94	34.68	15.70	12.69	19.63	12.69	39.50	74.68	35.99	1.51	45.50	53.03	45.78	32.09
AdaKV	16.83	25.08	36.52	45.79	35.94	15.06	12.97	19.40	12.97	42.50	76.67	36.46	2.73	47.00	53.54	45.54	32.81
ThinK	18.65	28.98	39.41	51.50	<u>39.33</u>	19.25	14.72	20.81	14.53	44.50	80.45	38.43	0.93	<u>85.50</u>	55.67	48.79	37.59
Snap+Zip	18.22	<u>31.79</u>	<u>46.14</u>	<u>52.48</u>	<u>38.27</u>	<u>20.22</u>	20.43	21.16	<u>19.33</u>	<u>61.00</u>	<u>84.02</u>	<u>40.83</u>	<u>1.67</u>	60.29	60.95	51.23	<u>39.25</u>
RDKV	24.94	39.23	49.24	59.71	43.46	25.50	<u>20.01</u>	23.15	20.18	70.50	84.64	41.88	0.75	100.00	<u>60.43</u>	52.29	44.74
<i>Qwen3-4B-Instruct-2507, B_{total} = 128L</i>																	
SnapKV	21.46	31.15	43.96	53.83	40.79	22.12	15.77	21.90	16.16	51.50	83.44	39.72	1.30	93.03	59.07	50.75	40.37
AdaKV	23.78	31.71	45.03	<u>57.81</u>	40.54	23.84	16.40	22.70	16.45	56.50	81.10	40.47	<u>1.60</u>	<u>98.00</u>	60.64	51.76	41.77
ThinK	22.88	35.83	44.32	56.70	40.32	23.61	18.68	<u>22.77</u>	17.87	59.00	84.64	40.93	1.32	97.00	61.76	52.80	42.53
Snap+Zip	<u>23.84</u>	<u>38.35</u>	<u>48.62</u>	57.59	<u>41.88</u>	<u>24.04</u>	<u>23.43</u>	22.18	<u>21.62</u>	<u>68.50</u>	<u>85.73</u>	<u>42.24</u>	1.91	<u>98.00</u>	<u>62.43</u>	<u>53.41</u>	<u>44.61</u>
RDKV	26.79	41.89	49.87	59.14	42.95	26.02	24.01	23.39	22.46	74.00	86.53	43.00	1.25	100.00	63.10	53.48	46.12
<i>Qwen3-4B-Instruct-2507, B_{total} = 256L</i>																	
SnapKV	<u>25.92</u>	36.55	<u>48.56</u>	59.14	41.07	25.18	19.13	22.75	19.34	65.00	84.21	40.26	1.72	<u>99.75</u>	62.46	53.74	44.05
AdaKV	25.46	38.20	48.10	<u>59.34</u>	42.49	26.44	19.46	23.01	19.60	69.00	86.32	40.80	1.75	100.00	63.18	<u>55.07</u>	44.89
ThinK	25.30	39.37	46.06	59.10	42.73	25.10	21.58	<u>23.14</u>	20.80	68.50	86.58	41.22	<u>1.88</u>	100.00	<u>63.50</u>	55.32	45.01
Snap+Zip	24.21	<u>40.99</u>	48.26	58.93	<u>42.75</u>	24.22	25.96	22.62	<u>23.13</u>	<u>72.50</u>	87.13	<u>43.42</u>	1.90	99.50	63.77	54.68	<u>45.87</u>
RDKV	26.45	43.49	50.30	59.60	42.91	<u>25.52</u>	27.30	23.80	23.30	74.00	<u>87.03</u>	44.27	1.25	100.00	63.39	53.91	46.66
<i>Qwen3-4B-Instruct-2507, B_{total} = 512L</i>																	
SnapKV	26.57	39.86	<u>48.52</u>	<u>59.27</u>	<u>43.23</u>	<u>26.10</u>	23.00	22.74	21.67	70.00	87.95	41.81	<u>1.99</u>	100.00	64.72	56.35	45.86
AdaKV	<u>26.72</u>	40.87	48.17	59.10	42.93	26.61	23.28	22.58	21.54	70.50	87.15	42.20	1.78	100.00	64.69	56.58	45.92
ThinK	26.48	41.08	46.44	59.15	42.90	25.06	24.79	<u>23.38</u>	22.38	72.50	<u>87.64</u>	42.51	2.06	100.00	65.07	56.34	46.11
Snap+Zip	25.47	<u>42.27</u>	47.80	57.58	43.17	23.24	<u>28.44</u>	22.60	<u>23.79</u>	75.00	86.82	<u>43.79</u>	1.94	99.50	<u>65.03</u>	<u>56.52</u>	<u>46.44</u>
RDKV	27.75	43.89	49.81	59.97	43.87	25.37	30.07	23.67	24.00	<u>74.50</u>	86.73	44.60	0.50	100.00	63.29	54.42	47.03
<i>Qwen3-4B-Instruct-2507, B_{total} = 1024L</i>																	
SnapKV	27.80	42.45	48.56	59.01	43.04	<u>25.83</u>	26.55	23.26	22.91	72.50	87.44	42.80	1.83	100.00	64.83	56.65	46.59
AdaKV	<u>27.64</u>	42.54	<u>48.65</u>	59.57	43.31	26.35	26.75	23.02	23.16	74.00	88.08	43.49	1.60	100.00	<u>64.86</u>	57.44	<u>46.90</u>
ThinK	26.73	42.98	47.88	58.62	43.18	24.97	27.90	23.55	23.43	75.00	87.85	42.95	<u>1.97</u>	100.00	65.48	<u>57.04</u>	46.85
Snap+Zip	26.60	<u>43.46</u>	47.80	59.57	43.76	22.11	<u>29.78</u>	22.67	<u>23.84</u>	73.50	87.36	<u>44.65</u>	2.16	99.50	64.09	56.08	46.68
RDKV	27.35	44.36	50.40	<u>59.35</u>	43.63	24.87	30.91	<u>23.29</u>	24.45	<u>74.50</u>	87.26	45.24	0.75	100.00	62.86	54.61	47.12

G Additional Experiments on InfiniteBench

In this section, we present a detailed evaluation of RDKV on the InfiniteBench benchmark [50], which extends long-context evaluation to sequences exceeding 100k tokens. The 10 tasks span three categories: (i) retrieval—Passkey Retrieval (Retr.Pass), Number Retrieval (Retr.Num), and KV Retrieval (Retr.KV)— which test the ability to locate and extract specific information embedded in long contexts; (ii) language understanding—English Dialogue (En.Dia), English Summarization (En.Sum), English Multiple-Choice (En.MC), English QA (En.QA), and Chinese QA (Zh.QA)— which evaluate comprehension and reasoning over novel-length inputs; and (iii) structured reasoning—Math Find (Math.Find) and Code Debugging (Debug)—which require precise numerical or logical retrieval. These tasks collectively pose challenges for both context retention and fine-grained information extraction at extreme sequence lengths.

We evaluate RDKV on LLaMA-3.1-8B-Instruct with $B_{\text{total}} = 1024L$. The evaluation compares RDKV with SnapKV, AdaKV, ThinK, SnapKV+ZipCache, and FullKV (oracle).

As reported in Tab. 11, RDKV achieves the highest average (39.46) among all compression methods, leading AdaKV (38.06) by 1.40 points. A breakdown by task category reveals where the advantage concentrates. On the retrieval tasks, RDKV scores 7.20 on KV Retrieval vs. ≤ 2.20 for all baselines—a $3.3\times$ improvement—because the needle-style retrieval pattern aligns directly with the rate-distortion allocation: high-attention tokens are preserved at high precision while low-attention tokens are aggressively quantized or removed. On language understanding tasks, RDKV leads on En.Dia (13.00 vs. ≤ 11.50), En.Sum (25.13 vs. ≤ 23.66), and En.QA (14.49 vs. ≤ 13.43), matching FullKV

Table 8: Performance on 16 LongBench datasets for LLaMA-2-13B-Chat and Qwen2.5-72B-Instruct (2-GPU tensor parallelism) at $B_{\text{total}} \in \{128L, 512L\}$. Snap+Zip denotes SnapKV+ZipCache. The best result in each row is in **bold**; the second-best is underlined.

Method	Single-Doc QA			Multi-Doc QA			Summarization			Few-shot Learning			Synthetic		Code		Avg.
	NrivQA	Qasper	MF-en	HotpotQA	2WikiMQA	Musique	GovRep	QMSum	MultiNews	TREC	TriviaQA	SAMSum	PCount	PRE	Lcc	RB-P	
<i>LLaMA-2-13B-Chat, $B_{\text{total}} = \text{Full}$</i>																	
FullKV	16.25	17.54	27.88	14.81	14.97	6.31	27.47	20.58	26.12	69.00	87.83	38.12	2.91	12.38	51.17	51.91	30.33
<i>LLaMA-2-13B-Chat, $B_{\text{total}} = 128L$</i>																	
SnapKV	13.96	16.25	25.98	15.90	14.40	<u>5.78</u>	19.40	20.07	20.52	41.00	86.12	34.97	2.78	12.13	46.23	44.95	26.28
AdaKV	14.71	17.81	28.54	16.27	15.12	5.52	19.71	20.19	21.51	<u>62.50</u>	87.02	34.93	<u>3.06</u>	10.25	49.59	48.58	28.46
ThinK	14.35	14.81	26.36	<u>16.29</u>	14.35	5.54	19.95	<u>20.24</u>	21.53	48.00	87.01	35.45	2.67	12.25	48.02	46.59	27.09
Snap+Zip	16.75	15.93	<u>27.73</u>	16.40	13.94	5.61	21.66	18.93	<u>23.18</u>	58.00	87.49	<u>35.79</u>	5.90	17.38	50.33	47.14	28.88
RDKV	<u>16.03</u>	<u>16.40</u>	27.09	15.17	<u>15.01</u>	6.89	22.42	20.29	24.10	68.50	<u>87.05</u>	36.86	3.01	<u>13.88</u>	<u>49.83</u>	50.73	29.58
<i>LLaMA-2-13B-Chat, $B_{\text{total}} = 512L$</i>																	
SnapKV	<u>15.57</u>	16.55	28.23	15.49	15.15	6.24	22.52	20.13	24.04	67.50	86.53	38.47	<u>3.09</u>	13.88	50.49	50.36	29.64
AdaKV	15.53	17.10	28.45	15.84	15.14	6.38	22.98	20.68	24.22	69.50	87.11	37.52	2.42	13.12	49.50	51.25	29.80
ThinK	15.52	<u>17.64</u>	<u>28.49</u>	<u>16.12</u>	14.88	<u>6.29</u>	23.16	19.95	24.52	68.00	86.75	37.97	2.84	13.88	50.10	50.60	29.79
Snap+Zip	13.18	14.74	28.41	17.03	13.03	5.84	<u>24.33</u>	<u>20.29</u>	<u>25.32</u>	<u>68.50</u>	86.76	<u>38.19</u>	5.50	9.50	49.65	50.99	29.45
RDKV	16.35	18.08	28.78	15.23	15.10	6.19	25.54	<u>20.27</u>	25.84	<u>68.50</u>	87.39	37.41	2.68	<u>13.12</u>	50.00	52.67	30.20
<i>Qwen2.5-72B-Instruct (2-GPU TP), $B_{\text{total}} = \text{Full}$</i>																	
FullKV	32.21	49.59	51.88	65.26	65.51	41.37	34.00	24.35	24.74	78.00	91.76	47.87	21.50	99.50	66.36	71.42	54.08
<i>Qwen2.5-72B-Instruct (2-GPU TP), $B_{\text{total}} = 128L$</i>																	
SnapKV	28.76	32.00	46.33	62.37	62.21	36.60	20.94	21.38	17.90	53.00	90.26	40.81	23.00	97.42	59.07	63.89	47.25
AdaKV	<u>30.68</u>	33.07	49.54	<u>63.92</u>	62.93	38.35	21.80	22.02	18.46	61.50	90.91	42.15	21.50	<u>99.25</u>	59.94	65.71	48.86
ThinK	28.02	29.54	46.30	62.17	61.47	37.73	20.72	21.27	17.70	47.00	90.28	40.22	21.50	96.17	58.42	63.51	46.38
Snap+Zip	30.60	46.38	50.50	65.47	64.97	40.35	<u>26.64</u>	<u>22.30</u>	22.14	<u>73.00</u>	<u>91.86</u>	45.29	19.50	99.00	64.03	68.52	51.91
RDKV	31.76	<u>44.79</u>	<u>49.57</u>	63.86	<u>64.42</u>	<u>39.72</u>	26.93	23.49	<u>22.10</u>	76.00	92.16	<u>45.15</u>	<u>22.00</u>	99.50	65.48	69.80	52.30
<i>Qwen2.5-72B-Instruct (2-GPU TP), $B_{\text{total}} = 512L$</i>																	
SnapKV	32.50	45.81	51.23	64.56	64.39	40.55	26.89	23.24	22.07	75.50	92.16	45.03	<u>21.50</u>	99.50	65.04	69.95	52.49
AdaKV	33.78	45.16	50.82	63.96	<u>64.80</u>	<u>40.83</u>	27.41	23.02	22.29	<u>76.50</u>	91.89	45.60	22.00	99.50	<u>65.48</u>	<u>70.48</u>	52.72
ThinK	31.03	43.89	50.81	<u>64.59</u>	64.58	39.35	26.33	23.42	21.92	73.50	<u>92.19</u>	45.76	21.00	<u>99.17</u>	65.34	69.89	52.05
Snap+Zip	32.50	50.24	51.80	64.21	64.33	41.00	<u>31.63</u>	<u>23.87</u>	24.23	78.00	92.61	<u>46.28</u>	<u>21.50</u>	99.50	65.03	69.85	53.54
RDKV	<u>32.65</u>	<u>49.51</u>	<u>51.68</u>	64.77	64.95	40.41	31.78	24.21	<u>23.94</u>	78.00	92.06	47.91	<u>21.50</u>	99.50	66.34	71.90	53.82

accuracy on En.MC (68.56). On structured reasoning tasks (Math.Find, Debug), all compression methods cluster near each other, indicating that cache compression is not the bottleneck once the relevant information is preserved.

H Additional Experiments on Ablation Study

H.1 Prefill Overhead

Tab. 12 breaks down the time-to-first-token (TTFT) for RDKV on LLaMA-3.1-8B-Instruct with a 128K-token prefill on a single A100 64GB. The baseline is a standard FullKV prefill with FlashAttention-2. RDKV bypasses the HuggingFace generate wrapper and calls transformer layers directly, saving 593 ms of framework overhead. The four RDKV-specific stages—weight computation (w_t, w_c), MCKP bisection, and TriZone packing—add a combined 2,331 ms. The net overhead is 1,740 ms, or 6.0% of the FullKV prefill, yielding a measured TTFT of 30,583 ms. This one-time cost is amortised over the entire decode sequence; with 128K context and the $4.5\times$ decode speedup reported in Sec. 4, RDKV breaks even within the first ~ 50 generated tokens.

H.2 K/V Budget Split Ratio

The main experiments fix an equal K/V split ($B^V = B^K = \frac{1}{2}B_{\text{head}}$) as a design convention (Sec. B). To validate this choice, we sweep the K budget ratio $r_K \in \{0.4, 0.5, 0.6\}$ (so $B^K = r_K B_{\text{head}}$ and $B^V = (1 - r_K)B_{\text{head}}$) on LLaMA-3.1-8B-Instruct at three cache budgets $B_{\text{total}} \in \{128L, 256L, 512L\}$. All other settings (observation window $S_w = 32$, pooling kernel $w = 5$, $B = \{0, 2, 4, 8, 16\}$) are kept identical.

Table 9: Performance on the 11 RULER tasks across context lengths $\{4k, 8k, 16k, 32k, 64k, 128k\}$ for LLaMA-3.1-8B-Instruct at $B_{\text{total}} = 2048L$. The best result in each row is in **bold**; the second-best is underlined. FullKV (no compression) is reported as a reference upper bound and excluded from the ranking.

Method	S-NIAH-1	S-NIAH-2	S-NIAH-3	MK-NIAH-1	MK-NIAH-2	MK-NIAH-3	MQ-NIAH	MV-NIAH	VT	CWE	FWE	Avg.
<i>Sequence length = 4k</i>												
FullKV	100.00	100.00	100.00	100.00	100.00	99.80	99.80	99.70	99.96	98.92	86.20	98.58
SnapKV	100.00	100.00	100.00	100.00	99.60	95.80	99.70	<u>99.70</u>	99.92	97.42	76.40	97.14
AdaKV	100.00	100.00	100.00	100.00	99.80	<u>99.00</u>	<u>99.75</u>	99.75	99.96	98.20	81.40	97.99
ThinK	100.00	100.00	100.00	100.00	<u>99.80</u>	96.80	99.70	99.50	99.80	99.12	<u>84.47</u>	<u>98.11</u>
Snap+Zip	46.60	98.60	92.80	99.80	63.00	0.00	99.20	94.65	88.40	83.72	74.60	76.49
RDKV	100.00	100.00	100.00	100.00	100.00	99.80	99.80	<u>99.70</u>	99.96	<u>98.94</u>	86.27	98.59
<i>Sequence length = 8k</i>												
FullKV	100.00	100.00	100.00	99.80	99.80	99.80	99.70	99.50	99.76	93.76	95.60	98.88
SnapKV	100.00	100.00	98.20	99.80	99.60	69.40	99.90	99.20	99.80	77.68	86.60	93.65
AdaKV	100.00	100.00	<u>96.60</u>	99.80	99.80	<u>86.20</u>	<u>99.80</u>	<u>99.35</u>	<u>99.76</u>	77.22	88.93	<u>95.50</u>
ThinK	100.00	100.00	92.80	99.80	99.80	67.00	99.65	99.20	<u>99.76</u>	<u>90.48</u>	<u>89.07</u>	94.32
Snap+Zip	66.00	98.80	88.60	99.00	69.80	0.00	98.15	92.70	73.56	65.96	81.73	75.85
RDKV	100.00	100.00	100.00	99.80	99.80	99.60	99.70	99.50	<u>99.76</u>	93.54	95.53	98.84
<i>Sequence length = 16k</i>												
FullKV	100.00	100.00	100.00	100.00	100.00	99.80	99.70	98.70	99.68	73.38	95.53	96.98
SnapKV	100.00	99.80	94.60	99.60	100.00	45.60	99.75	<u>98.90</u>	99.32	<u>54.84</u>	<u>94.33</u>	89.70
AdaKV	100.00	100.00	<u>96.00</u>	99.40	100.00	<u>67.60</u>	99.80	98.70	99.52	46.32	93.00	<u>90.94</u>
ThinK	100.00	100.00	80.20	100.00	99.00	38.20	99.80	99.00	99.20	54.28	90.93	87.33
Snap+Zip	47.60	98.00	82.80	99.20	55.80	0.00	95.05	92.35	73.32	36.42	76.47	68.82
RDKV	100.00	100.00	100.00	100.00	99.80	99.00	99.60	98.65	99.52	77.26	95.07	97.17
<i>Sequence length = 32k</i>												
FullKV	100.00	100.00	100.00	99.40	99.60	99.20	99.60	99.20	99.04	10.18	87.40	90.33
SnapKV	100.00	98.80	94.60	98.80	99.20	32.60	99.40	<u>98.50</u>	96.60	21.12	72.93	82.96
AdaKV	100.00	98.60	<u>95.00</u>	99.20	99.60	49.80	99.55	98.40	<u>97.68</u>	20.28	68.33	<u>84.22</u>
ThinK	100.00	100.00	76.80	99.40	95.20	21.20	99.35	97.95	97.12	18.16	68.33	79.41
Snap+Zip	94.60	100.00	90.80	99.00	46.40	1.80	<u>99.50</u>	95.95	83.28	<u>21.26</u>	<u>76.13</u>	73.52
RDKV	100.00	100.00	99.80	99.40	<u>99.40</u>	90.60	99.30	98.55	98.52	23.98	79.67	89.93
<i>Sequence length = 64k</i>												
FullKV	100.00	100.00	100.00	99.40	98.40	97.00	99.05	94.50	96.64	1.22	87.13	88.49
SnapKV	100.00	94.80	89.80	98.60	96.20	13.00	98.15	<u>94.15</u>	89.80	2.64	<u>80.00</u>	77.92
AdaKV	100.00	95.40	92.60	98.60	94.40	<u>21.80</u>	<u>98.50</u>	93.85	<u>91.84</u>	2.28	76.73	<u>78.73</u>
ThinK	100.00	97.00	70.40	<u>99.00</u>	83.40	5.20	98.45	94.00	90.80	2.14	67.67	73.46
Snap+Zip	99.60	100.00	<u>94.60</u>	<u>99.00</u>	42.60	0.80	98.30	92.10	84.00	4.66	85.33	72.82
RDKV	100.00	<u>99.20</u>	99.80	99.40	<u>95.40</u>	56.40	99.45	94.45	94.44	<u>3.58</u>	73.13	83.20
<i>Sequence length = 128k</i>												
FullKV	100.00	99.40	99.80	97.60	88.60	66.20	98.45	90.65	66.56	0.00	71.80	79.91
SnapKV	100.00	99.20	50.80	97.20	82.20	3.20	<u>97.10</u>	90.25	<u>66.60</u>	<u>0.12</u>	<u>52.20</u>	67.17
AdaKV	100.00	99.20	47.80	97.20	74.40	<u>5.40</u>	97.15	89.15	63.16	0.10	35.00	64.42
ThinK	100.00	99.20	61.80	97.00	<u>81.60</u>	2.00	96.10	88.70	62.96	0.18	49.00	67.14
Snap+Zip	100.00	96.20	<u>85.40</u>	95.00	49.00	1.80	92.05	81.30	67.32	0.06	63.87	66.55
RDKV	100.00	99.00	93.80	96.80	<u>81.60</u>	9.00	96.45	88.50	63.12	0.06	44.73	70.28

Tab. 13 reports the 16-task LongBench average. At every budget level the equal split $r_K = 0.5$ achieves the highest score. The margins are small (≤ 0.63 points), indicating that the allocation is robust to moderate shifts in the K/V ratio. Shifting more budget toward K ($r_K = 0.6$) consistently hurts: the V cache carries per-token information that directly scales the attention output (Prop. 3.1), so starving it degrades quality faster than under-provisioning per-channel K precision. Conversely, a mild reduction of K budget ($r_K = 0.4$) is largely absorbed because the per-channel distortion weight w_c (Prop. 3.2) concentrates on a small subset of outlier channels; most channels tolerate lower bit-widths with negligible error. The symmetric optimum $r_K = 0.5$ balances these two effects, justifying the equal split adopted throughout the paper.

Table 10: RDKV vs. HqeKV [17] on the 11 RULER tasks across context lengths {16k, 32k, 64k} for LLaMA-3.1-8B-Instruct at $B_{\text{total}} = 1024L$. The best result in each row is in **bold**.

Method	S-NIAH-1	S-NIAH-2	S-NIAH-3	MK-NIAH-1	MK-NIAH-2	MK-NIAH-3	MQ-NIAH	MV-NIAH	VT	CWE	FWE	Avg.
<i>Sequence length = 16k</i>												
HqeKV	100.00	99.40	99.00	99.60	99.80	86.40	96.70	95.10	96.20	26.80	95.00	90.40
RDKV	100.00	99.80	100.00	99.60	99.60	86.20	99.40	98.50	99.20	76.70	93.20	95.70
<i>Sequence length = 32k</i>												
HqeKV	99.80	99.20	88.80	96.60	98.60	85.20	93.80	91.00	95.30	15.30	87.20	86.40
RDKV	100.00	98.40	99.60	98.40	98.80	71.20	99.20	98.30	98.70	37.30	71.20	88.30
<i>Sequence length = 64k</i>												
HqeKV	99.60	96.00	72.40	97.20	94.80	28.00	86.40	81.00	86.20	0.10	84.10	75.10
RDKV	100.00	98.40	99.00	99.00	93.00	30.60	98.60	93.00	92.90	6.60	69.70	80.10

Table 11: Performance on the 10 InfiniteBench tasks for LLaMA-3.1-8B-Instruct at $B_{\text{total}} = 1024L$. The best result among compression methods is in **bold**; the second-best is underlined. FullKV is reported as a reference upper bound.

Method	Retr.Pass	Retr.Num	Retr.KV	En.Dia	En.Sum	En.MC	En.QA	Zh.QA	Math.Find	Debug	Avg.
FullKV	100.0	99.32	56.20	18.00	27.52	68.56	14.63	13.28	34.00	22.34	45.38
SnapKV	100.00	<u>96.61</u>	1.40	8.50	23.35	<u>68.12</u>	12.58	<u>12.44</u>	34.00	22.08	37.91
AdaKV	100.00	94.41	1.80	10.50	<u>23.66</u>	<u>68.12</u>	12.94	12.30	34.00	22.84	<u>38.06</u>
ThinK	100.00	87.97	1.80	7.00	23.03	<u>68.12</u>	11.21	12.35	<u>33.71</u>	22.08	36.73
Snap+Zip	100.00	91.86	<u>2.20</u>	<u>11.50</u>	22.16	67.69	<u>13.43</u>	12.40	34.00	22.34	37.76
RDKV	100.00	96.95	7.20	13.00	25.13	68.56	14.49	12.65	34.00	<u>22.59</u>	39.46

Table 12: Prefill overhead breakdown for RDKV on LLaMA-3.1-8B-Instruct at 128K context length (A100 64 GB). Percentages are relative to the FullKV prefill baseline.

Component	Time (ms)	% of FullKV Prefill
FullKV prefill (FA2)	28 843	— (baseline)
Forward path saving	-593	-2.1%
w_t computation	+308	+1.1%
w_c computation	+550	+1.9%
MCKP bisection	+609	+2.1%
TriZone packing	+863	+3.0%
Net RDKV overhead	+1,740	+6.0%
RDKV TTFT	30 583	106.0%

I Visualization of Bit Allocation

To illustrate how the RDKV allocator distributes bit-widths across tokens and channels, we visualize the per-unit distortion weight w_t (V cache, Prop. 3.1) and w_c (K cache, Prop. 3.2) together with the resulting bit-width assignment $b \in \{0, 2, 4, 8, 16\}$ on a representative LongBench sample (LLaMA-3.1-8B-Instruct, $B_{\text{total}} = 128L$). Each dot is coloured by its assigned bit-width: ● 16-bit, ● 8-bit, ● 4-bit, ● 2-bit; tokens assigned 0 bits (evicted) are omitted. We show layers 15 (middle) and 31 (final) with two KV heads each.

Token-level V allocation (Fig. 7–Fig. 13). The score distribution spans roughly six orders of magnitude. Sink tokens (position 0) and recent tokens near the sequence tail consistently receive the highest scores and correspondingly 16-bit or 8-bit retention—the former carry accumulated attention mass, and the latter fall within the observation window. The bulk of mid-sequence tokens reside at 2–4 bits. Head 0 and head 1 share the global profile but differ in which mid-sequence positions spike, reflecting head-specific attention patterns.

Table 13: K/V budget split ablation: per-task LongBench scores for LLaMA-3.1-8B-Instruct at $B_{\text{total}} \in \{128L, 256L, 512L\}$. r_K denotes the fraction of B_{head} allocated to K. The best result in each row is in **bold**; the second-best is underlined.

r_K	Single-Doc QA				Multi-Doc QA			Summarization			Few-shot Learning			Synthetic		Code		Avg.
	NrivQA	Qasper	MF-en	HotpotQA	2WikiMQA	Musique	GovRep	QMSum	MultiNews	TREC	TriviaQA	SAMSum	PCount	Pre	Lec	RB-P		
<i>LLaMA-3.1-8B-Instruct, $B_{\text{total}} = 128L$</i>																		
$r_K=0.4$	29.65	41.93	56.21	<u>56.51</u>	48.05	30.93	25.58	24.98	24.37	<u>63.50</u>	92.14	41.11	8.58	99.50	61.09	53.55	<u>47.36</u>	
$r_K=0.5$	<u>29.45</u>	<u>41.34</u>	<u>55.55</u>	57.39	49.38	<u>30.89</u>	<u>25.55</u>	<u>24.59</u>	<u>24.29</u>	65.00	91.92	41.80	8.75	100.00	62.68	55.41	47.75	
$r_K=0.6$	29.22	38.60	55.40	56.47	<u>48.69</u>	30.74	24.69	24.12	23.44	<u>63.50</u>	<u>91.94</u>	<u>41.61</u>	8.75	100.00	62.41	54.92	47.15	
<i>LLaMA-3.1-8B-Instruct, $B_{\text{total}} = 256L$</i>																		
$r_K=0.4$	29.22	<u>43.75</u>	<u>56.13</u>	56.89	49.16	30.85	28.26	24.74	25.71	67.00	<u>91.61</u>	41.19	8.52	99.50	63.11	53.89	48.10	
$r_K=0.5$	29.63	44.85	56.33	57.85	49.64	31.73	<u>28.01</u>	24.66	<u>25.66</u>	70.00	91.87	<u>41.79</u>	8.83	99.50	63.27	<u>56.01</u>	48.73	
$r_K=0.6$	29.15	43.62	55.49	<u>57.05</u>	<u>49.21</u>	<u>31.28</u>	27.09	24.89	25.28	<u>68.50</u>	91.20	42.77	<u>8.68</u>	100.00	62.54	56.51	<u>48.33</u>	
<i>LLaMA-3.1-8B-Instruct, $B_{\text{total}} = 512L$</i>																		
$r_K=0.4$	29.85	<u>45.35</u>	56.77	57.04	48.99	31.11	30.72	25.24	<u>26.37</u>	70.50	91.91	42.26	8.75	100.00	63.41	55.73	49.00	
$r_K=0.5$	30.24	45.67	55.58	<u>57.06</u>	<u>48.95</u>	<u>31.67</u>	<u>30.68</u>	<u>25.06</u>	26.46	72.00	<u>91.83</u>	43.15	8.83	100.00	63.36	<u>57.02</u>	49.22	
$r_K=0.6$	<u>29.92</u>	44.96	<u>55.61</u>	57.31	48.78	31.97	29.78	24.93	26.29	<u>71.00</u>	91.58	<u>43.02</u>	8.93	99.50	63.38	57.17	<u>49.01</u>	

Channel-level K allocation (Fig. 8–Fig. 14). The 128 channels of each head display a heavy-tailed score distribution. A small number of outlier channels—typically 2–4 per head—receive 16-bit, with scores 2–3 orders of magnitude above the median. These correspond to the persistent outlier channels documented in prior work on KV cache quantization [13, 12]: the product $\|Q_{:,c}\|_2 \|K_{:,c}\|_2$ is dominated by a handful of dimensions where both query and key norms are large. The allocator automatically assigns these channels full precision while compressing the remaining channels to 4–8 bits, avoiding the uniform-precision penalty that affects fixed-bit-width quantization methods.

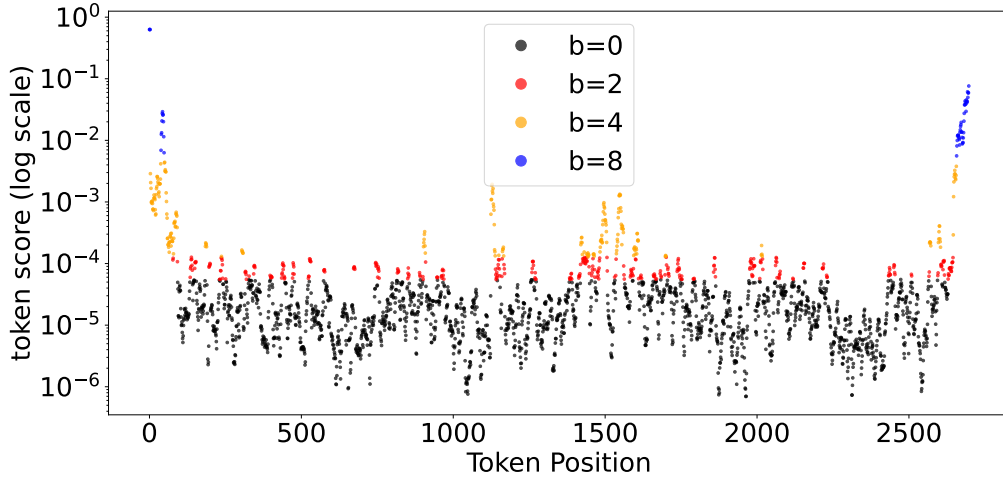


Figure 7: Per-token V-cache bit allocation: layer 15, head 0.

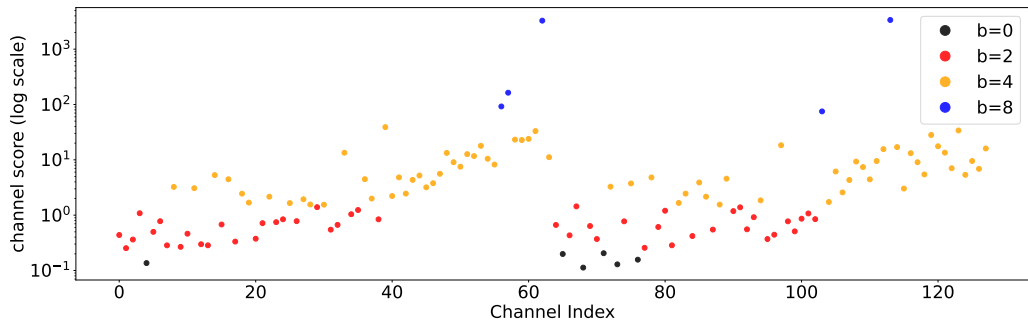


Figure 8: Per-channel K-cache bit allocation: layer 15, head 0.

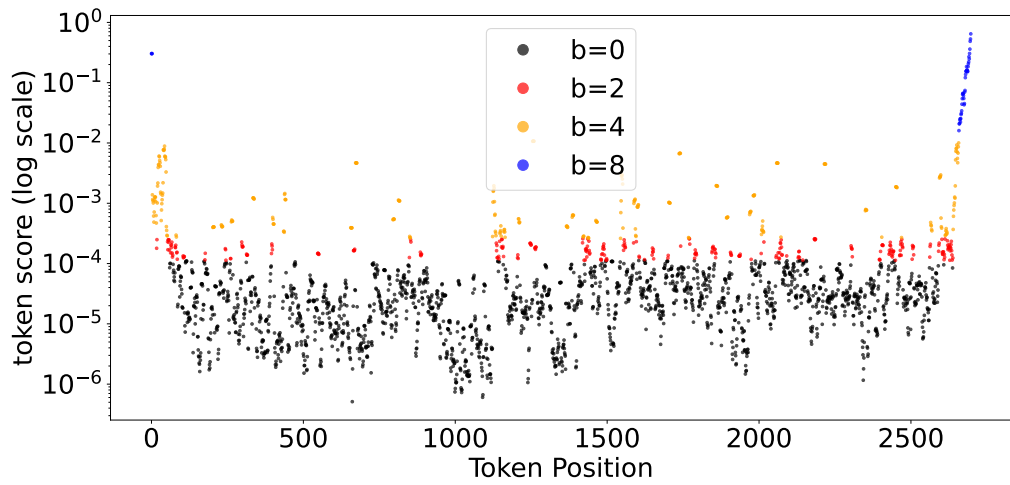


Figure 9: Per-token V-cache bit allocation: layer 15, head 1.

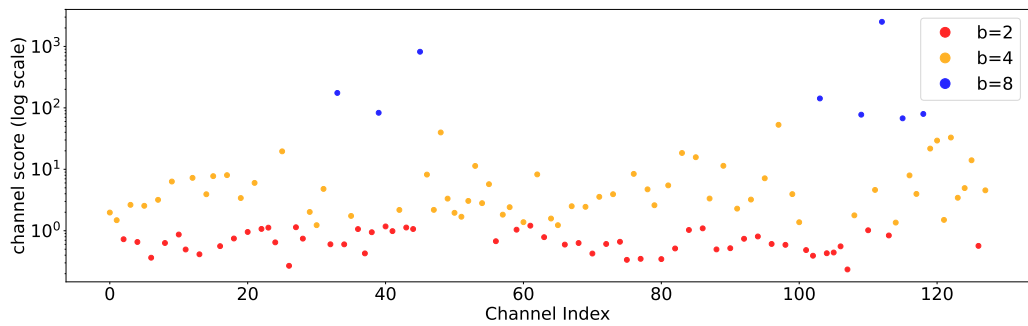


Figure 10: Per-channel K-cache bit allocation: layer 15, head 1.

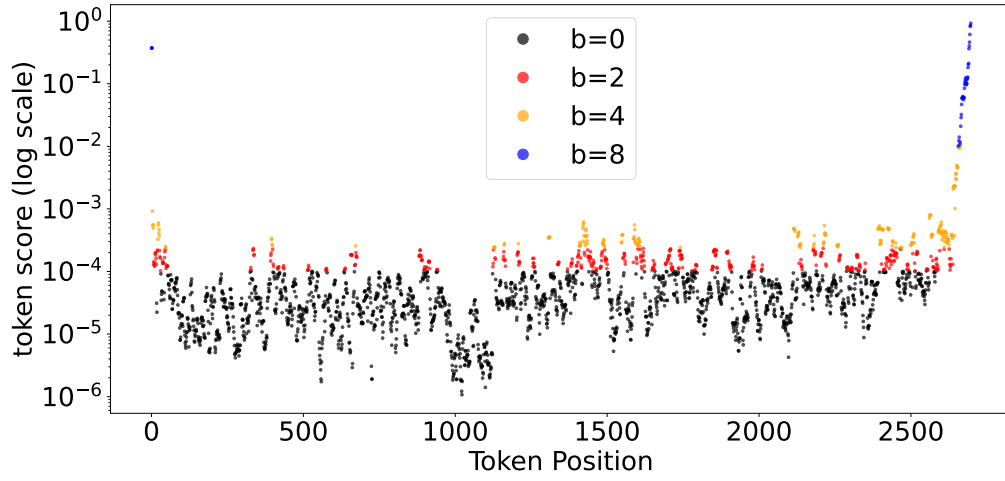


Figure 11: Per-token V-cache bit allocation: layer 31, head 0.

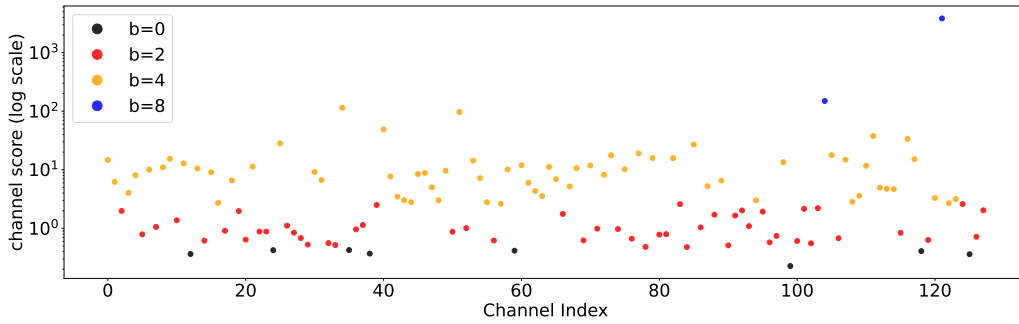


Figure 12: Per-channel K-cache bit allocation: layer 31, head 0.

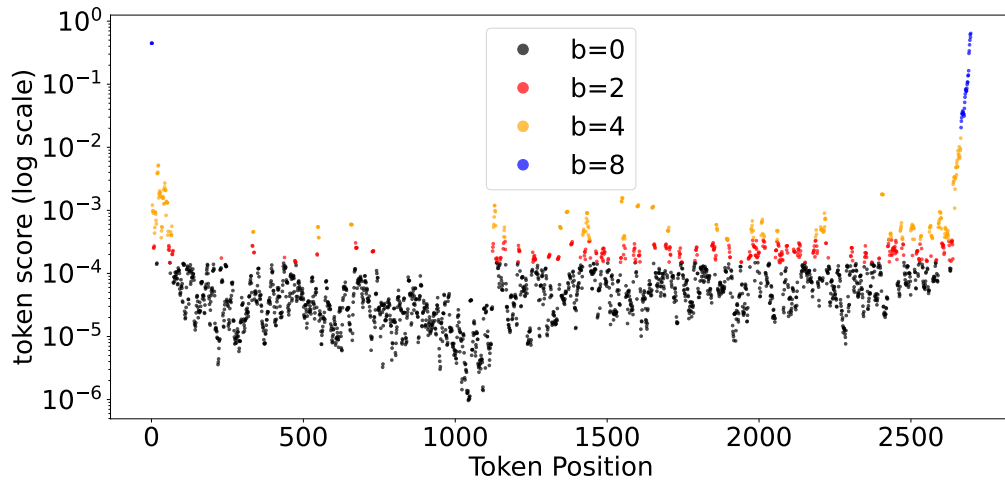


Figure 13: Per-token V-cache bit allocation: layer 31, head 1.

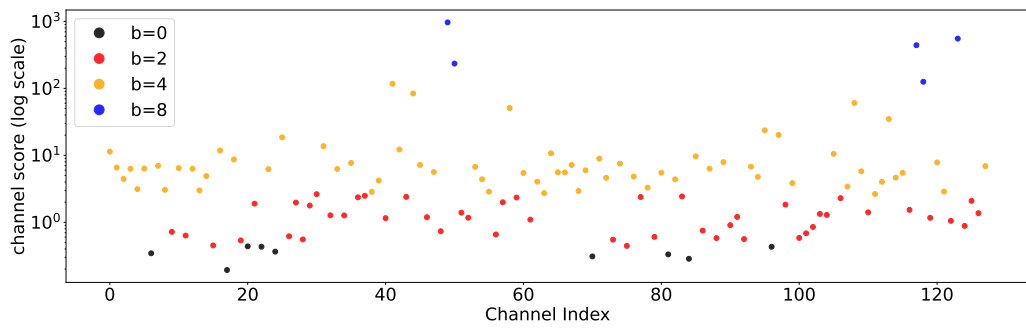


Figure 14: Per-channel K-cache bit allocation: layer 31, head 1.

J Calibrated Distortion Tables

Table 14 reports the calibrated per-coordinate distortion $\varepsilon^K(b)$ (K cache, per-channel NMSE) and $\varepsilon^V(b)$ (V cache, per-token NMSE) for each evaluated model and bit-width $b \in \{2, 4, 8\}$. Each entry is averaged across all layers, heads, and 32 calibration sequences (4 k tokens, LongBench prefill prefixes; see Sec. B for calibration details). These layer-averaged values are the distortion tables consumed by the MCKP solver (Prop. A.3). All models share $\varepsilon(0) = 1$ (eviction) and $\varepsilon(16) = 0$ (full precision).

V cache distortion is notably consistent across architectures at every bit-width, whereas K cache distortion shows greater cross-model variance—chiefly because Qwen2.5-72B’s embedding-adjacent layers exhibit elevated per-channel 8-bit quantization error.

Table 14: Calibrated normalized distortion $\varepsilon(b)$ per model. K cache: per-channel NMSE; V cache: per-token NMSE.

Model	$\varepsilon^K(b)$ (per-channel)			$\varepsilon^V(b)$ (per-token)		
	$b=2$	$b=4$	$b=8$	$b=2$	$b=4$	$b=8$
LLaMA-3.1-8B	0.149	0.0062	2.2×10^{-5}	0.313	0.0140	4.9×10^{-5}
LLaMA-2-13B	0.288	0.0124	5.5×10^{-5}	0.272	0.0122	4.4×10^{-5}
Mistral-7B	0.280	0.0116	6.9×10^{-5}	0.296	0.0130	4.5×10^{-5}
Qwen2.5-72B	0.296	0.0164	4.4×10^{-3}	0.281	0.0126	4.4×10^{-5}
Qwen3-4B	0.347	0.0147	1.5×10^{-4}	0.313	0.0139	4.8×10^{-5}

K Limitations and Future Work

Limitations. Like SnapKV, AdaKV, and PyramidKV, RDKV compresses the KV cache once after prefill and does not re-evaluate during decoding. This is a common design choice in the prefill-dominated regime (long prompt, short generation) targeted by these methods. The allocation is therefore frozen with respect to attention-pattern shifts that may occur during generation.

Future work. The rate-distortion framework can be extended to the decode phase. A natural approach accumulates attention weights over a small buffer of recent decode tokens and periodically applies the same MCKP allocation to compress them, keeping decode-phase memory sub-linear in the number of generated tokens relative to the uncompressed baseline.

L Impact Statement

RDKV reduces the memory footprint and decoding latency of long-context LLM inference without modifying model weights or training procedures. On the positive side, lower hardware requirements enable longer context windows on smaller GPUs, reducing both the financial cost and the energy consumption of serving long-context applications such as document summarization, multi-document QA, and retrieval-augmented generation. This may broaden access to long-context LLM capabilities for resource-constrained practitioners and organizations. More broadly, by reducing the number of GPU hours required per query, RDKV lowers the energy consumption and carbon footprint of LLM serving, contributing to more environmentally sustainable deployment of long-context inference. On the negative side, as with any inference acceleration technique, reduced serving cost could lower the barrier to deploying LLMs at scale, potentially amplifying existing concerns associated with large-scale LLM deployment such as misinformation generation. However, RDKV does not introduce new model capabilities—it preserves the output distribution of the original model within the compression budget—and therefore does not create risks beyond those already present in the underlying LLM.